

1    **Monitoring of greenhouse gases and pollutants across an urban**  
2    **area using a light-rail public transit platform**

3  
4    Logan E. Mitchell<sup>1,\*</sup>, Erik T. Crosman<sup>1</sup>, Alexander A. Jacques<sup>1</sup>, Benjamin Fasoli<sup>1</sup>, Luke Leclair-  
5    Marzolf<sup>1</sup>, John Horel<sup>1</sup>, David R. Bowling<sup>2</sup>, James R. Ehleringer<sup>2</sup>, John C. Lin<sup>1</sup>

6  
7    <sup>1</sup> Department of Atmospheric Sciences, University of Utah, Salt Lake City, UT

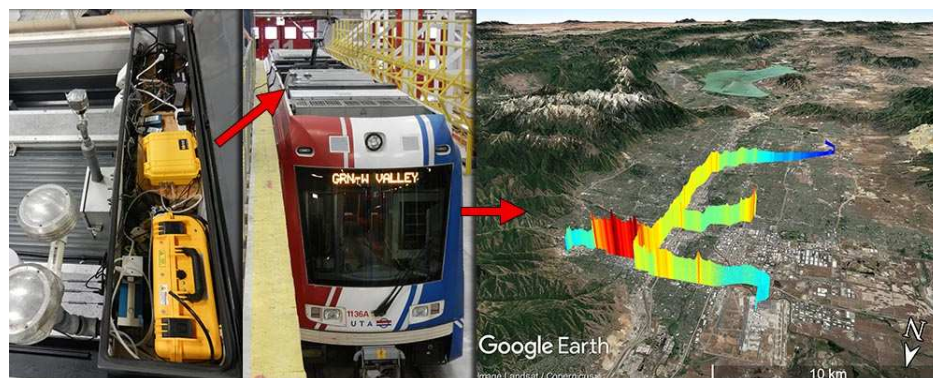
8    <sup>2</sup> Department of Biology, University of Utah, Salt Lake City, UT

9    \* Corresponding author. E-mail address: [logan.e.mitchell@gmail.com](mailto:logan.e.mitchell@gmail.com) (L. Mitchell)

10  
11    **Keywords:** urban atmosphere; greenhouse gas; air pollution; spatial pattern; temporal pattern;  
12    mobile monitoring

13  
14    **Declarations of interest:** none

15  
16    **Graphical Abstract:**



20 **Abstract**

21 Anthropogenic emissions within urban environments are characterized by spatial  
22 heterogeneity and temporal variability that present challenges for measuring urban greenhouse  
23 gases and air pollutants. To address these challenges, we mounted instruments on public transit  
24 light-rail train cars that traverse the metropolitan Salt Lake Valley (SLV) in Utah, USA to  
25 observe the temporal and spatial variability of atmospheric species including carbon dioxide  
26 ( $\text{CO}_2$ ), methane ( $\text{CH}_4$ ), ozone ( $\text{O}_3$ ), fine particulate matter ( $\text{PM}_{2.5}$ ), and nitrogen dioxide ( $\text{NO}_2$ ).  
27 Utilizing electrified light-rail public transit as an observational platform enables real-time  
28 measurements with low operating costs while avoiding self-contamination from vehicle exhaust.  
29 We examine temporal averages and case studies of each species that reveal gradients,  
30 intermittent point sources, seasonal and diel changes, and complex relationships resulting from  
31 emissions, atmospheric chemistry, and meteorological conditions.  $\text{CO}_2$  and  $\text{NO}_2$  are related  
32 through the combustion of fossil fuel and we observed a broad spatial gradient across the city as  
33 well distinct plumes at traffic intersections and, for  $\text{NO}_2$ , a large plume adjacent to a locomotive  
34 rail yard. Distributions of  $\text{O}_3$  were strongly correlated with  $\text{NO}_2$  due to atmospheric  
35 photochemical and titration processes. Episodes of high  $\text{PM}_{2.5}$  had distinct spatial patterns  
36 depending on meteorological conditions during wintertime persistent cold-air pool episodes. The  
37 spatial pattern of  $\text{CH}_4$  was characterized by distinct plumes associated with industrial and  
38 commercial facilities, some of which followed temporal patterns indicative of daytime working  
39 hours; other plumes were persistent throughout the whole day, suggestive of leak-related fugitive  
40 emissions. The ongoing multi-year record of spatial and temporal air quality observations  
41 provides a valuable data set for future air quality exposure studies. Our results suggest pollution  
42 and greenhouse gas emission monitoring and exposure assessment could be greatly enhanced by  
43 deploying instruments on public transit systems in urban centers worldwide.

44

45

46

## 47 **1. Introduction**

48 Trace species in the atmosphere have a wide range of impacts including climate change,  
49 health, and ecosystem impacts. Metropolitan areas are characterized by concentrated emissions  
50 and large intra-urban spatiotemporal variability of greenhouse gases (GHGs) and pollutants  
51 (Baldauf et al., 2008; Christen et al., 2011). Poor urban air quality leads to impacts on human  
52 health (e.g. respiratory, circulatory, cancer, mortality, etc. (Di et al., 2017; Landrigan et al.,  
53 2017)) as well as cascading economic impacts (e.g. health care costs, decreased worker  
54 productivity, etc. (Zivin and Neidell, 2018)) and environmental impacts (e.g. O<sub>3</sub> injury to plants,  
55 viewshed impacts from haze, etc. (U.S. EPA, 2013)). Detailed observations and models are  
56 needed to resolve the intra-urban environment in order to link human health impacts to pollutant  
57 variability and to investigate the anthropogenic, chemical, and meteorological factors controlling  
58 the variability in urban GHGs and pollutants as cities are growing (Gurney et al., 2015; Park and  
59 Kwan, 2017; Venkatram et al., 2009). While models of emissions have improved in temporal and  
60 spatial resolution (e.g. (Gurney et al., 2009; Hoek et al., 2008; Pouliot et al., 2012) the ability of  
61 current urban monitoring networks to provide constraints for these models remains limited (Air  
62 Quality Research Subcommittee, 2013; Hutyra et al., 2014).

63 Currently, numerous observational configurations exist to monitor ambient concentrations of  
64 trace species across urban areas for research or regulatory purposes. Examples include monitors  
65 for U.S. Environmental Protection Agency (US EPA) Criteria Air Pollutants to comply with the  
66 regulatory requirements of the Clean Air Act, or the National Oceanic and Atmospheric  
67 Administration's Global Greenhouse Gas Reference Network that is used to conduct research on  
68 the global carbon cycle. These observations, located at fixed sites, have been maintained for  
69 decades with high precision and accuracy, and have resulted in numerous insights into health  
70 consequences of pollutants (Correia et al., 2013) or the impacts of trace species on global climate  
71 (Le Quéré et al., 2016). However, sparse networks of stationary sites are intended to monitor air  
72 quality across large spatial scales (regional or counties) and cannot resolve spatial  
73 heterogeneities that are known to exist within urban environments.

74 As atmospheric monitoring instrumentation decreases in size and cost, the paradigm for  
75 urban air monitoring has evolved to include higher spatial resolution (Kumar et al., 2015; Snyder  
76 et al., 2013). It has become possible to deploy dense networks of temporary or permanent fixed  
77 sites that can resolve intra-urban spatial patterns (e.g., (Deville Cavellin et al., 2016; Jiao et al.,

78 2016; Matte et al., 2013; Shusterman et al., 2016). These dense networks typically consist of  
79 many instruments that present maintenance and calibration challenges over time (Borrego et al.,  
80 2016; Kelly et al., 2017; Miskell et al., 2016; Thompson, 2016). In the last several years, a  
81 proliferation of low-cost sensors driven by citizen science initiatives and the rapid development  
82 of micro-sensor technology has dramatically increased air quality data collection across urban  
83 landscapes, but more research on how to calibrate these low-cost sensors with research-grade  
84 instrumentation is needed (Barakeh et al., 2017; Clements et al., 2017; Zimmerman et al., 2017).  
85 Assessing intra-urban spatial patterns has also been undertaken for research applications by  
86 deploying sensors on mobile platforms (Gozzi et al., 2016) such as automobiles, aircraft, and  
87 bicycles (e.g., (Apte et al., 2017; Hopkins et al., 2016; Lee et al., 2017; Mays et al., 2009; Van  
88 den Bossche et al., 2015). While mobile platforms improve spatial coverage, labor costs are often  
89 considerable, limiting the long-term deployability of such mobile platforms. Hence, it is difficult  
90 to conduct manned mobile monitoring campaigns to assess changes over time or to characterize  
91 the impact of intermittent emissions on ambient concentrations without considerable cost. While  
92 both mobile and stationary sampling approaches have benefits and challenges, a well-defined  
93 best practice for sustained monitoring at fine scales of urban atmospheric trace species has  
94 remained elusive.

95 Here we present a new project that facilitates routine real-time monitoring of intra-urban  
96 atmospheric trace species using research grade instruments mounted on public transit light-rail  
97 vehicles that transect the Salt Lake Valley (SLV) metropolitan area at routine intervals. To our  
98 knowledge, only a few mobile urban observation networks leveraging public transit currently  
99 exist worldwide: Zurich, Switzerland (Hasenfratz et al., 2015); Karlsruhe, Germany (Hagemann  
100 et al., 2014); Oslo, Norway (Castell et al., 2015); and Perugia, Italy (Castellini et al., 2014). Each  
101 of these projects have different experimental designs with a different suite of measurements, and while  
102 their utility is still being explored, it has been shown that public transit based monitoring can be used to  
103 create high-resolution maps of air pollution across urban areas (Hasenfratz et al., 2015). Our study is  
104 the first effort to utilize public transit for urban observations of trace species in North America.  
105 Starting in December 2014, we partnered with the Utah Transit Authority (UTA) and installed  
106 instrumentation to measure carbon dioxide (CO<sub>2</sub>), methane (CH<sub>4</sub>), ozone (O<sub>3</sub>), and fine  
107 particulate matter (PM<sub>2.5</sub>) in a secure box on the roof of an electrically-powered light-rail public  
108 transit train (aka “TRAX”). A second suite of sensors on another TRAX train car was added in

109 February 2016. Basic meteorological parameters (temperature, relative humidity, and pressure)  
110 were also measured. Additionally, temporary installations of instruments that measure black  
111 carbon and nitrogen dioxide (NO<sub>2</sub>) were deployed for short periods. To facilitate public  
112 engagement, real-time data were transmitted to University of Utah servers every five minutes  
113 and made accessible via web-based visualizations (<http://air.utah.edu/> and  
114 <http://meso1.chpc.utah.edu/mesotrax/>).

115 The SLV, with a population of just over 1 million people, experiences on average 40 days  
116 annually of pollutant levels (including both summer and winter pollutant episodes) exceeding the  
117 U.S. National Ambient Air Quality Standards (NAAQS) resulting from a combination of  
118 meteorological patterns, topography, and emissions. In the winter, elevated levels of PM<sub>2.5</sub> result  
119 from emissions accumulating in persistent cold air pools (PCAPs; locally known as temperature  
120 inversions). On average, 6.8 PCAPs occurred each winter, with an average duration of 3.1 days,  
121 that exceeded the NAAQS for PM<sub>2.5</sub> of 35 µg m<sup>-3</sup> on average 18 days per winter, however with  
122 considerable interannual variability (Whiteman et al., 2014). During winter, the maximum  
123 (minimum) temperatures were 3.5 (-6) °C and average snowfall was 110 cm. The snow cover  
124 reflected incoming radiation, maintaining cool surface temperatures and enhanced nocturnal  
125 surface radiative cooling, resulting in stronger wintertime PCAPs when snow cover was present.  
126 During summer the average maximum (minimum) temperatures were 32 (16) °C, but there were  
127 frequent high-pressure ridges over the Western US that resulted in prolonged periods of elevated  
128 heat and stagnation. These meteorological conditions, in combination with urban precursor  
129 emissions and wildfire smoke, led to the photochemical production of elevated ground level O<sub>3</sub>  
130 that exceeded the NAAQS for O<sub>3</sub> of 70 ppb on average 22 days per year (Horel et al., 2016).  
131 Public awareness of the health risks associated with summertime O<sub>3</sub> is less than for wintertime  
132 PM<sub>2.5</sub> because O<sub>3</sub> is invisible, and high concentrations are often accompanied by fair weather.  
133 Episodic air quality reductions also result from dust storms and wild fires several times each year  
134 (Mallia et al., 2017, 2015; Steenburgh et al., 2012). As a result of all of these factors, intense  
135 public interest in improving air quality exists, as demonstrated by the 2016 Utah Foundation  
136 survey of voter's concerns that found air quality among the public's most pressing issues  
137 (Bateman et al., 2016). Finally, because of the number of NAAQS exceedances, The Utah  
138 Division of Air Quality (DAQ) is currently engaged in developing a State Implementation Plan  
139 (SIP) to improve air quality to bring the state into compliance with the Clean Air Act.

140 In addition to air quality concerns, Salt Lake City has adopted aggressive greenhouse gas  
141 emission reduction targets (Salt Lake City Corporation, 2016) that, if successful, will result in  
142 observable reductions in concentrations of GHGs in the city in the coming years. Many other  
143 public and private stakeholders are also engaged in GHG mitigation efforts as well.

144 Several complimentary resources are available that could assist in evaluating and utilizing the  
145 TRAX based observations. These include a high-density meteorological observation network  
146 (Horel et al., 2016), a GHG monitoring network (Mitchell et al., 2018), a growing low-cost  
147 citizen-science led network of air quality monitors (Kelly et al., 2017)  
148 (<https://www.purpleair.com/>), a small network of research-grade fixed air quality monitoring  
149 stations (Baasandorj et al., 2017), and detailed emissions models (Patarasuk et al., 2016). The  
150 combination of poor air quality, wide ranging interest from the public, stakeholders,  
151 governments and regulators, as well as several complimentary resources make the SLV a unique  
152 testbed for evaluating a public transit based atmospheric observation system (Lin et al., in press).

153 In this paper our main goal is to provide an overview of an ongoing light-rail public transit-  
154 based observation project that has measured air pollutants and GHGs across an urban area at  
155 high resolution for the past 3 years. We describe our experimental design, present examples of  
156 how these observations can be utilized, and discuss future directions for mobile observations  
157 deployed on public transit platforms.

158

## 159 **2. Materials and Methods**

### 160 **2.1. TRAX Light Rail Network**

161 The SLV contains the state capital, Salt Lake City, and is located within Salt Lake County,  
162 Utah in the inter-mountain west of the continental U.S. (Figure 1). It is bounded by the Wasatch  
163 and Oquirrh Mountains on the east and west sides of the valley, the Traverse Mountains to the  
164 south, and the Great Salt Lake to the northwest. The TRAX light rail train network consists of  
165 over 145 electric trains servicing three lines (Red, Green, and Blue) along 94 km of rail track that  
166 provide coverage across the SLV (Figure 1). Urbanization along the rail lines varies from dense  
167 urban downtown regions to suburban and rural settings, and the train travels on and off major  
168 roadways. TRAX operates an older model of rail car on the Blue line, so our data are almost  
169 exclusively from the Red and Green lines. Along the Red and Green lines there are 25 and 18  
170 passenger stops, and it takes 60 and 46 minutes, respectively, to complete a transect on each line.

171 In addition to the spatial coverage, the Red line also provides a 225 m pseudo-vertical profile  
172 from the valley floor (1,285 m) to the surrounding mountain foothills (1,510 m). Each TRAX  
173 train car covers 18-24 transects when operating for a full day (approximately 18 hours from 5  
174 AM to midnight). During the period December 2014 – April 2017, the trains have been deployed  
175 760 days comprising 10,300 transects (averaging 14 transects a day and deployed 61% of days,  
176 or ~4 days a week). When the trains were not in operation, they were often parked outside and  
177 therefore became periodic stationary observation sites that provided additional observations.  
178 Several complementary stationary GHG and air pollutant stations were located in close  
179 proximity to the TRAX route that can be used to evaluate the TRAX based measurements. This  
180 includes the DAQ Hawthorne site as well as several University of Utah air quality and GHG  
181 monitoring sites (Figure 1).

182

## 183 **2.2. Instrumentation Set-up**

184 Two TRAX trains (numbered 1136 and 1104, hereafter TRAX 1 and 2) were outfitted with  
185 sensors to measure air quality, GHGs, and meteorological parameters. Electrified trains are an  
186 ideal platform for air sampling because they have zero direct emissions and often run  
187 continuously throughout the day. The trains have electric circuitry on their roofs in steel  
188 weatherproof boxes, and our instruments were installed in one of the spare boxes (dimensions  
189 1.5 m x 0.5 m x 0.5 m). The sample inlets extended 0.5 m above the top of the train through a  
190 pipe protruding from the metal box topped with a vent cover and were 4 m above ground level.  
191 AC power was provided with a connection into the cabin accessory outlets. Two generic  
192 computer fans provided cooling for the instruments in the box in the summer. Table 1 lists the  
193 equipment installed on the TRAX trains, their sampling frequency, and their measurement  
194 accuracy as reported by the equipment manufacturers. The Campbell Scientific CS215-L  
195 Temperature and Relative Humidity probe and CS106 Barometer were used for the  
196 meteorological parameters. Data were recorded by a Raspberry Pi based data logger (which also  
197 controlled a valve systems for hourly automated GHG calibrations) and a Campbell Scientific  
198 data logger (CR1000). The observations were transmitted to University of Utah servers via  
199 cellular communications every 5 minutes. Figure 2 summarizes the temporal data coverage by  
200 species between the start of the project through April 2017. Gaps in the data resulted from a  
201 variety of factors including train maintenance, instrument maintenance, and periods when

202 instrument calibration parameters were unknown or unavailable (Figure 2). A greater number of  
203 train transects per month occurred when we requested enhanced observations during intensive  
204 field campaigns (e.g., summer 2015 and winter 2017), while decreased numbers of train transects  
205 per month occurred when the trains were undergoing maintenance.

206 To examine the mean variability in GHG and air pollutants over various time periods (e.g.,  
207 average summertime O<sub>3</sub>, or annual GHGs), we calculated averages along the rail track using  
208 available transects during these periods. This was carried out by creating a track of  
209 approximately equally spaced (~35-40 m) points along each of the train lines. Then for each  
210 transect of the train from one end of a line to the other, the data were assigned to the nearest  
211 equally spaced point along the track. Since the spacing of the points is suited for a 1-Hz sampling  
212 frequency, we linearly interpolated the observations from the E-Sampler and 2B Ozone monitors  
213 to a 1-Hz sampling rate. If there were multiple observations at a single point (e.g. during a 45  
214 second stop at a station where passengers boarded the train), the observations were averaged,  
215 resulting in equal spatial extent for data along each train transect. These transects could then be  
216 averaged over selected temporal periods to create a spatially explicit, temporally averaged  
217 composite of the data.

218 In order to correctly interpret the spatial observations, the GPS location data must be  
219 precisely synchronized with the atmospheric measurements. A time lag between the GPS and  
220 other measurements can arise from a misalignment in the clocks, but this was addressed by  
221 recording a common time stamp from the data logger to all of the data files. A secondary time  
222 lag can result from the amount of time it takes for a parcel of air to travel the length of the inlet  
223 tubing to the instrument. This was addressed empirically by identifying stationary features in the  
224 data (point source emissions, freeway, etc.) and specifying a time lag such that the feature occurs  
225 in the same place when the train was traveling in both directions (Figure 3). This led to a higher  
226 correlation between data averaged when the train was traveling in both directions. Time lags  
227 varied between instruments and with changes in tubing but were in the range of 1-15 seconds.

228 Calibration of the GHG measurements was conducted hourly using a working reference gas  
229 tank with known near ambient CO<sub>2</sub> and CH<sub>4</sub> mole fractions tertiary to the World Meteorological  
230 Organization X2007 CO<sub>2</sub> mole fraction scale (Zhao and Tans, 2006) and the NOAA04 CH<sub>4</sub> mole  
231 fraction scale (Dlugokencky et al., 2005). The ozone monitors, which have been approved by US  
232 EPA as a Federal Equivalent Method (FEM), were calibrated from either the manufacturer or at a



233 DAQ facility, while the PM<sub>2.5</sub> sensors were calibrated by the manufacturer approximately  
234 annually. The NO<sub>2</sub> analyzer has an internal metal oxide scrubber that produces NO<sub>2</sub>-free air that  
235 provides a zero calibration every 30 minutes that were subtracted from the observations. Since  
236 this instrument was installed temporarily, the NO<sub>2</sub> span was only calibrated twice during the  
237 year-long deployment with two different sets of calibration equipment. In both cases there was  
238 an excellent linear response ( $R^2 > 0.99$ ) but the slope of the line at the start of the deployment  
239 was 1.07 and at the end it was 0.88. We did not correct for this change over time because of the  
240 infrequency of the span calibrations and because of the different calibration equipment used.  
241 Thus, while there is likely a  $\pm 10\%$  uncertainty in the absolute magnitude of the NO<sub>2</sub>  
242 observations, prior work has found that the span changes slowly over time (Brent et al., 2013), so  
243 the relative magnitude of the spatial patterns across the city are robust.

244

### 245 **2.3. Evaluation against stationary sites**

246 To evaluate our mobile measurements, we compared the TRAX observations to observations  
247 made at two stationary measurement sites located near the TRAX train lines (Figure 4). We  
248 evaluated the TRAX observations against the Utah Division of Air Quality (DAQ) Hawthorne  
249 site maintained by the state of Utah for US EPA regulatory purposes that is 2 km east of the train  
250 line along a section where the Red and Green lines overlap, as well as the University of Utah  
251 (UOU) site located 0.6 km north of the TRAX Red line in the northeast part of the SLV (Figure  
252 1). The goal was to provide representative comparisons and an overall sense of the robustness of  
253 the TRAX data. Future work should include more detailed comparisons and include fixed sites  
254 co-located next to the TRAX train line, depending on species of interest.

255 For PM<sub>2.5</sub> we compared the TRAX observations against the hourly DAQ measurements that  
256 utilized a FEM for the month of February 2016. This time period was chosen because there was a  
257 persistent cold air pool (PCAP) event and PCAP events tend to have a large dynamic range in  
258 PM<sub>2.5</sub> and often do not have fine scale spatial variability (Baasandorj et al., 2017), as discussed  
259 in the PM<sub>2.5</sub> results section below. Thus, for this time period, the TRAX measurements should be  
260 comparable to those at the DAQ monitoring station 2 km east of the train line. The TRAX  
261 observations were averaged over a 2.3 km long section of the train line as well as subsections  
262 where the train was moving and where it was stopped at two train stops. While the temporal  
263 spans of the measurements were different (a few minutes on TRAX vs. hourly average at DAQ),

264 this was the most accessible comparison to evaluate the TRAX measurements against a FEM  
265 monitoring station. We observed a good correlation for most of the month (circles); however, in  
266 the middle of the PCAP event the ambient relative humidity (RH) increased and caused the  
267 TRAX instruments to record anomalously high PM<sub>2.5</sub> concentrations (triangles), due to  
268 hygroscopic swelling of particles, causing the nephelometer to overestimate the PM<sub>2.5</sub>  
269 concentration. The MetOne PM<sub>2.5</sub> analyzers on the two trains both use onboard heaters to dry the  
270 air prior to measurement and we have found that they are unable to suitably dry the air when  
271 ambient relative humidity is greater than ~85%. These high relative humidity conditions were  
272 infrequent and are easily identified by comparisons with the DAQ monitor, so they did not pose  
273 a problem for our experimental design and we have removed these periods from the data set. The  
274 good agreement with high R<sup>2</sup> values during normal operations exist regardless of whether the  
275 train was in motion or stationary, indicating that our experimental setup was not sensitive to the  
276 speed of the train (not shown).

277 For O<sub>3</sub> and NO<sub>2</sub> we also compared the TRAX measurements to the hourly DAQ  
278 measurements. We examined these relationships for the entire year NO<sub>2</sub> measurements were  
279 available (June 2016-June 2017) but found that the slope of the relationships changed during the  
280 winter, when oxidant titration could at times lead to complete titration of O<sub>3</sub> (Baasandorj et al.,  
281 2017). Therefore, we excluded the winter months (November-February) from the comparison.  
282 For this comparison we again found high correlations (R<sup>2</sup> ≥ 0.8) that give confidence in the  
283 TRAX-based mobile observations.

284 For the GHGs we compared the TRAX measurements and those at the UOU site during a  
285 time period with good data coverage from June-October, 2015. We averaged the TRAX  
286 observations over a 1-km section of the track and compared them to the UOU observations over  
287 the same time period (~50 second duration). Both CO<sub>2</sub> and CH<sub>4</sub> measurements had high  
288 correlations (R<sup>2</sup> > 0.8), indicating good overall agreement. The scatter in the comparisons is  
289 likely due to the proximity of local sources (traffic and fugitive CH<sub>4</sub> emissions).

290

### 291 **3. Results and Discussion**

292 In the following sections, we provide examples of the observed variations in GHGs and  
293 criteria pollutants observed with the TRAX platform. Human and natural factors such as  
294 emissions from on-road, industrial and residential sources, as well as chemical processes,

295 meteorology, and topography affect the observed concentrations. The complex wind flow  
296 patterns and vertical stability owing to the unique meteorology and topography of the SLV  
297 control to a large degree the transport and mixing of trace species in the boundary-layer. The  
298 daily cycle of heating and cooling in a mountain valley combined with thermal contrasts between  
299 the Great Salt Lake and the SLV results, in the absence of strong winds associated with synoptic  
300 weather systems, in down-valley flow (from south to north) at night and up-valley flow (from  
301 north to south) during the day throughout the year (Blaylock et al., 2016; Crosman and Horel,  
302 2016; Horel et al., 2016). These thermally-driven circulation patterns combine with terrain-flow  
303 interactions (Lareau and Horel, 2015, 2014) and variations in boundary-layer depth (Whiteman  
304 et al., 2014; Young and Whiteman, 2015) to impact pollutant variability across the SLV. In  
305 addition, emissions and chemical reactions (e.g., point sources and the distance to roadway)  
306 within the complex urban landscape also drive patterns in trace species (Horel et al., 2016). All  
307 of the data shown in the figures and the native Google Earth KMZ files are included in the  
308 Supplementary Materials.

### 309 **3.1. Greenhouse Gases**

#### 310 **3.1.1. Carbon Dioxide (CO<sub>2</sub>)**

311 The average CO<sub>2</sub> mole fractions in the SLV from available transects during the duration of  
312 the project (December 2014-April 2017) shows spatial patterns across roadway, neighborhood,  
313 and urban scales (Figure 5a). Across the metropolitan region, CO<sub>2</sub> mole fractions were higher in  
314 the urban center and along the north-south urban corridor in the center of the SLV while lower  
315 mole fractions were visible along the urban periphery and were lowest in the southwestern SLV  
316 near the edge of the suburban margin of the urbanized area. This mole fraction gradient pattern  
317 (sometimes referred to as an ‘urban dome’ (Idso et al., 2001); however this terminology can be  
318 misinterpreted because the measurements are all at the surface and do not characterize vertical  
319 distributions) was created by the density of emissions from the on-road, residential, commercial,  
320 and industrial sectors across the urban landscape. The SLV has one of the longest running multi-  
321 site urban CO<sub>2</sub> monitoring networks in the world, consisting of five sites that began operation in  
322 2001 (Mitchell et al., 2018), which can be compared to the TRAX spatiotemporal averages.  
323 While the broad structure of the urban gradient across the SLV is observable at the fixed sites,  
324 the TRAX observations resolve the spatial structure of mole fraction gradients across the  
325 metropolitan region in much finer detail than is possible from a small number of fixed sites.

326 In addition to the broad spatial pattern across the city, there were smaller-scale features that  
327 were visible in the averages. Elevated CO<sub>2</sub> mole fractions were found along every road that the  
328 train crosses. On the Red line between the urban center and the University of Utah (2.5 to 6.5 km  
329 along the Red line in Figure 5), the rail tracks were located in the middle of a four-lane road with  
330 heavy automobile traffic (>20,000 vehicles day<sup>-1</sup> in 2014 (UDOT, 2017)) and surrounded by  
331 multi-story buildings that act as an urban canyon and could reduce ground level atmospheric  
332 mixing. This combination of factors resulted in the highest CO<sub>2</sub> mole fractions we observed  
333 along the TRAX lines. In other areas, the train ran on a dedicated transit corridor that was not  
334 adjacent to tailpipe emissions, was in the vicinity of roads with less traffic, or was surrounded by  
335 shorter buildings, and these factors resulted in lower CO<sub>2</sub> mole fractions.

336 One advantage of using a transit-based observation platform is its ability to make repeated  
337 transects on a regular basis that provides unprecedented temporal coverage for a mobile  
338 platform. With this data we can examine the spatial pattern of CO<sub>2</sub> mole fractions during  
339 different seasons (Figure 5b), days of the week (Figure 5c), and hours of the day (Figure 5d).  
340 These comparisons reveal higher mole fractions at night and during the winter months due to  
341 lower planetary boundary layers during these time periods and, during the winter, greater  
342 emissions from combustion of natural gas for home heating (Mitchell et al., 2018; Pataki et al.,  
343 2003). Lower mole fractions during the day were caused by greater atmospheric mixing as well  
344 as photosynthetic uptake of CO<sub>2</sub> from vegetation. The magnitude of the seasonal and diel cycles  
345 were much larger along the urban corridor where there were greater anthropogenic emissions  
346 than there were at the southwestern end of the Salt Lake Valley at the margin of the urbanized  
347 area (~35 km in Figure 5b). The mole fractions along the urban corridor (10 to 27 km in Figure  
348 5c) were also higher during the week than during the weekend due to greater levels of traffic, but  
349 this difference was not as large in the downtown core of the city (5 to 7.5 km in Figure 5c).  
350 These examples illustrate the rich temporal coverage that is possible with a public-transit based  
351 measurement platform.

352

### 353 **3.1.2. Methane (CH<sub>4</sub>)**

354 Numerous studies have documented CH<sub>4</sub> leaks across urban areas tied to industrial activities,  
355 natural gas infrastructure, and landfills (e.g. (Hopkins et al., 2016; Jackson et al., 2014; Lamb et  
356 al., 2016; McKain et al., 2015)). In the SLV, the averaged CH<sub>4</sub> mole fractions from available

357 transects were characterized by distinct plumes, in contrast to the broad pattern of CO<sub>2</sub> (Figure  
358 6). A number of the CH<sub>4</sub> plumes are adjacent to industrial sources including natural gas fired  
359 power plants and a brick factory that utilizes a natural gas turbine to fire its furnace, as well as  
360 landfills.

361 An analysis of CH<sub>4</sub> during different hours of the day demonstrates the ability of a public  
362 transit platform to identify intermittent emission sources (Figure 6b). While the CH<sub>4</sub> plume near  
363 the brick factory (marked by an 'K' in Figure 6b) and natural gas fired power plant ('P' in Figure  
364 6b) along the Red line are present throughout the day, there is one plume ('X' in Figure 6b) that  
365 was only present during daytime working hours, indicating a source of methane likely related to  
366 commercial or manufacturing activity. Mobile measurement campaigns that only make a few  
367 passes by any particular source (e.g. using a vehicle (Hopkins et al., 2016)) or that only operate  
368 during certain times of day or on specific days (e.g. (Apte et al., 2017) could miss intermittent  
369 sources such as those that are only present during specific times of the day or those with episodic  
370 day-to-day variability.

371

## 372 **3.2. Air Pollutants**

### 373 **3.2.1. Fine Particulate Matter (PM<sub>2.5</sub>)**

374 Events when PM<sub>2.5</sub> concentrations exceed NAAQS in the SLV are highly episodic, so more  
375 insight can be gained by looking at specific case studies than by examining average conditions  
376 over time until numerous episodes are available to derive a climatology of various episodes (the  
377 three-year record is insufficient at this point). In January-February 2016 a study was conducted  
378 that examined how meteorological and chemical processes affected wintertime PM<sub>2.5</sub> during  
379 persistent cold air pools (PCAPs) (Baasandorj et al., 2017), and the TRAX observations provide  
380 additional insight into the spatial variability during this study. Figure 7 shows several 4-hr PM<sub>2.5</sub>  
381 averages along the Red line during the 7-15 February 2016 pollution episode, which contained  
382 eight consecutive daily NAAQS exceedances of PM<sub>2.5</sub>. Near the beginning of this episode on 8  
383 February 2016 a pronounced north-south gradient in PM<sub>2.5</sub> was observed along the Red line  
384 (Figure 7a). Meteorological observations from MesoWest stations ((Horel et al., 2002); Figure  
385 1), laser ceilometers, and lidar data from field campaigns (Baasandorj et al., 2017) as well as  
386 stationary air quality sites were utilized determine the cause of this gradient in PM<sub>2.5</sub> and  
387 indicated that it resulted from two factors. First, relatively clean and cool drainage flow through

388 the gap in the southern mountain foothills and downslope katabatic flows with wind speeds  
389 between 3 and 8 m s<sup>-1</sup> was observed at the southern end of the SLV that diluted the pollutants in  
390 those locales (indicated qualitatively with arrows in Figure 7a). Second, a weak northerly flow in  
391 the northern Salt Lake Valley resulting from a lake breeze circulation resulted in a stagnation  
392 zone (Crosman and Horel, 2016) over the northern and central SLV, allowing the PM<sub>2.5</sub>  
393 concentrations to remain elevated there. A small but distinct plume of ~20 µg m<sup>-3</sup> was observed  
394 in the south-central SLV adjacent to a gravel pit, indicated with a 'G' in Figure 7a. A week later,  
395 on the afternoon of 14 February 2016, near the end of the pollution episode, the spatial gradient  
396 in PM<sub>2.5</sub> had reversed, with PM<sub>2.5</sub> concentrations between 20 and 30 µg m<sup>-3</sup> higher over the  
397 southern portions of the SLV (Figure 7b). In this case a partial 'mix-out' episode (Lareau and  
398 Horel, 2014) had partially removed the cold air and pollution in the Salt Lake Valley, but not in  
399 the Utah Valley. The stronger cold-air pool associated with colder temperatures over the Utah  
400 Valley to the south resulted in a density-driven flow of cold, polluted air that advected north into  
401 the SLV. Finally, in the evening of 14 February, top-down erosion of the PCAP (Lareau and  
402 Horel, 2014) led to a rapid decrease in PM<sub>2.5</sub> on the SLV benches on the north and southern ends  
403 of the TRAX Red line and left a shallow remnant polluted layer in the lowest ~150 m of the SLV  
404 (Figure 7c). Similar meteorological and pollution patterns were observed as part of an intensive  
405 field campaign during a PCAP in February 2017 (Utah DEQ, 2018).

406 Patterns visible in the TRAX data at other times (but not plotted here) include clean air  
407 drainage out of the surrounding canyons into the SLV and lake breezes that can transport either  
408 clean or polluted air into the city, depending on the composition of the air over the Great Salt  
409 Lake.

410 In the summer, average TRAX PM<sub>2.5</sub> concentrations were well below the NAAQS of 35 µg  
411 m<sup>-3</sup> (Figure 8). However studies have shown that adverse health effects can arise from even low  
412 pollutant concentrations (Brunekreef and Holgate, 2002; Di et al., 2017; Franklin et al., 2006)  
413 and near-road exposure to pollutants (Chen et al., 2017; Oakes et al., 2016). The TRAX average  
414 summer observations reveal numerous plumes of PM<sub>2.5</sub> associated with some roadways and  
415 several point sources (e.g. a gravel pit, brick factory, and an unidentified source, indicated by a  
416 'G', 'K', and 'X' in Figure 8).

417 While fine scale location-specific air quality forecasts will remain difficult to provide to the  
418 public, the observations from TRAX, in combination with a sparse network of fixed-site research

419 and regulatory instruments and citizen-science network of lower-cost sensors (Kelly et al., 2017),  
420 along with instruments deployed on a news helicopter (Crosman et al., 2017), provide DAQ  
421 forecasters with improved understanding of the complex intra-urban meteorological and  
422 topographical factors that control pollutant concentrations.

423

### 424 **3.2.2. Ozone (O<sub>3</sub>)**

425 Periods of high summertime O<sub>3</sub> are typically enhanced by stagnant high pressure and high  
426 temperature; however, there are also occasional episodic periods of high O<sub>3</sub> resulting from  
427 smoke from wildfires and lake breezes (Horel et al., 2016). The spatial patterns from summer-to-  
428 summer are similar, so we focus on the summer of 2015 that was investigated as part of the  
429 Great Salt Lake Summer Ozone Study (Blaylock et al., 2016; Horel et al., 2016). The average O<sub>3</sub>  
430 concentrations from available TRAX transects in the summer of 2015 were 5-10 ppb lower in the  
431 urban corridor compared to the foothills (Figure 9a). This pattern, however, changed throughout  
432 the day with midday concentrations being homogeneous across the city while the depletion in the  
433 urban corridor occurred entirely in the evening and morning hours when residual O<sub>3</sub> was  
434 preferentially destroyed by enhanced nocturnal NO<sub>x</sub> build-up in the urban corridor (Figure 9b).  
435 These distinct spatial patterns could allow for the comparison with spatial patterns in health  
436 impacts from O<sub>3</sub> that may lead to advances in understanding of O<sub>3</sub>-related health risks. In  
437 addition to the broad spatial patterns, areas of high-density traffic routes that are sources of NO<sub>x</sub>  
438 emissions from vehicles had sharp reductions in O<sub>3</sub> from near-field chemical destruction of O<sub>3</sub>  
439 that occurred throughout the day. These areas of depleted O<sub>3</sub> were evident along the freeways  
440 and are discussed in greater detail in the following sections.

441

### 442 **3.2.3. Nitrogen Dioxide (NO<sub>2</sub>)**

443 The average distribution of NO<sub>2</sub> across the SLV showed similar spatial patterns as CO<sub>2</sub> (r =  
444 0.83) and a strong anti-correlation with O<sub>3</sub> (Figure 10). The broad pattern shows NO<sub>2</sub>  
445 concentrations that were highest in the urban core and lowest along the urban periphery.  
446 Localized enhancements were visible along many of the roadways. These spatial patterns can be  
447 more clearly understood in relation to the other species that we measured, and a discussion of  
448 these relationships follows.

449

### 450 3.3. O<sub>3</sub>-NO<sub>2</sub>-CO<sub>2</sub> Relationships

451 Additional insight and an improved understanding of the factors controlling urban air  
452 composition can be gained by examining the relationships between several species (Figure 11).  
453 First, we discuss how O<sub>3</sub> and NO<sub>2</sub> are related through atmospheric chemistry; second, we  
454 examine the relationship between NO<sub>2</sub> and CO<sub>2</sub>, which are related through the combustion of  
455 fossil fuels.

456 The O<sub>3</sub>-NO<sub>2</sub> chemistry is well known (U.S. EPA, 2013), and the strong anti-correlation  
457 between O<sub>3</sub> and NO<sub>2</sub> ( $r = -0.96$ ) was a result of titration of O<sub>3</sub> by reaction with NO to form NO<sub>2</sub>  
458 ( $\text{NO} + \text{O}_3 \rightarrow \text{NO}_2$ ). This is particularly evident by examining the shaded regions of Figure 11  
459 where the train cars were in the middle of traffic in the downtown region (A), and crossed I-15,  
460 the major north-south interstate route in the SLV (B, C, and D). These instances reflect the  
461 atmospheric chemistry near highly-traveled roadways, but similar smaller features were observed  
462 near smaller roadways as well. These results, obtained with a single set of instruments, are  
463 similar to what would be expected from a large field campaign examining distance to road  
464 relationships, illustrating the utility of public transit platforms for urban air quality studies.  
465 Future work should add nitric oxide (NO) to the measurement suite to determine NO<sub>x</sub> ( $\equiv \text{NO} +$   
466  $\text{NO}_2$ ) and these observations could be used to improve our ability to model pollutants across the  
467 city and thereby improve high-resolution pollution exposure assessments. Understanding these  
468 processes will be important as energy efficiency and adoption of electric vehicles alter emissions  
469 patterns in urban centers. Prior modeling work has shown that future urban NO<sub>x</sub> emission  
470 reductions will lead to changes in the temporal patterns of urban O<sub>3</sub>, resulting in higher nighttime  
471 O<sub>3</sub> and lower daytime O<sub>3</sub> (Pfister et al., 2014), and the TRAX platform is well suited to observe  
472 these changes across an entire urban center in real time.

473 To explore the relationship between NO<sub>2</sub> and CO<sub>2</sub>, we calculated the excess NO<sub>2</sub> and CO<sub>2</sub>  
474 concentrations by subtracting a qualitative estimate of background conditions (4 ppb NO<sub>2</sub> and  
475 405 ppm CO<sub>2</sub>, slightly below the minimum in the spatial averages in Figure 11) and then  
476 calculating the excess NO<sub>2</sub>/CO<sub>2</sub> (ppb/ppm) ratio. Both NO (which is quickly titrated to NO<sub>2</sub> by  
477 O<sub>3</sub>) and CO<sub>2</sub> are co-emitted during the combustion of fossil fuels, but the ratio between them  
478 differs by source sector, fuel type, as well as vehicle speed, weight, age, and other factors (Jung  
479 et al., 2011). The impact of these differences can be most clearly seen by comparing the fine  
480 scale variations in the ratio in the shaded regions A-C in Figure 11. In region A the train was in



481 the middle of traffic on surface streets in downtown and the ratio was low. In contrast, in regions  
482 B and C where the train crossed the I-15 interstate with a different vehicle fleet composition  
483 moving at faster speeds, there were small peaks in the ratio. These observations provide useful  
484 targets for future work evaluating vehicle emissions in real world driving conditions and can also  
485 be compared to ratios measured at stationary tower sites during episodic periods of poor air  
486 quality (Bares et al., 2018).

487 Figure 12 shows an expanded view of the shaded region D from Figure 11 where a large  
488 persistently elevated NO<sub>2</sub> plume was seen. A close examination reveals that the NO<sub>2</sub> plume had  
489 two sub-peaks. The NO<sub>2</sub> peak at ~16.4 km where the Green line crossed I-15 was coincident  
490 with a narrow peak in CO<sub>2</sub>, and because there was a proportional increase in both species at this  
491 location there was a negligible effect on the excess NO<sub>2</sub>/CO<sub>2</sub> ratio (red shading). Conversely, the  
492 peak centered at ~16.8 km (blue line) is more clearly resolved in the excess NO<sub>2</sub>/CO<sub>2</sub> ratio that  
493 reveals a much larger and broader NO<sub>2</sub> plume and suggests that the NO<sub>x</sub> emissions from the  
494 freeway traffic were small compared to this other source. This second peak was centered over a  
495 Union Pacific rail yard 0.4 km west of the I-15 freeway that uses diesel powered switchyard  
496 locomotives to move rail cars around the rail yard (the location of the rail yard can be more  
497 clearly seen in the Google Earth KMZ supplementary materials). These switchyard locomotives  
498 comply with older (Tier 0 or 0+) locomotive emission standards (Sowards, G., personal  
499 communication, 2017) that have a high NO<sub>x</sub>/CO<sub>2</sub> emission ratio (U.S. EPA, 2016). The north-  
500 south extent of the excess NO<sub>2</sub>/CO<sub>2</sub> ratio can be observed along the Red line for ~6 km (between  
501 ~8-14 km, Figure 11). Since these values were averaged over an extended time period, it is  
502 expected that day-to-day wind conditions would spread this plume of higher NO<sub>2</sub> in different  
503 directions across the SLV. Upgrading the switchyard locomotives to newer models (Tier 4)  
504 would reduce NO<sub>x</sub> emissions by 90% and may be a cost-effective way to reduce emissions of  
505 this air pollutant (U.S. EPA, 2016).

506 These relationships illustrate the variety of impacts that fossil fuel combustion has on the  
507 composition of urban air. By measuring both GHGs and air pollutants, it will be possible to gain  
508 a greater understanding of the complex relationships between these species during different  
509 seasons and times of day as a result of emissions from anthropogenic and natural (e.g. biogenic)  
510 sources as well as secondary atmospheric chemical reactions. As efforts to improve air quality or  
511 reduce GHG emissions lead to lower emissions in urban centers, measurement platforms that

512 have the ability to monitor these species across space and time will be able to track the evolution  
513 of urban air composition across cities in a unique way.

514

### 515 **3.4. Future Directions**

516 We continue to collect data in real-time from the TRAX platforms. The long-term data  
517 archive, combined with other research and regulatory air quality observational networks, provide  
518 the opportunity to establish the Salt Lake Valley as an interdisciplinary laboratory for continued  
519 health science and air quality research that would benefit the public, urban planners, policy  
520 makers, and air quality forecasters. The research-grade instrumentation installed on the light rail  
521 train also has potential future value as a tethering system for calibrating lower-cost air quality  
522 sensors spatially distributed along the rail line. Utilizing public transit for urban atmospheric  
523 monitoring also provides a proof of concept that could be implemented in other urban regions  
524 throughout the world.

525 Disseminating real-time public transit air quality observations can be a powerful tool for  
526 science communication and could potentially boost public transit ridership. By taking public  
527 transit, customers can contribute to air quality monitoring while also reducing their own  
528 emissions and therefore improving air quality. Since ridership depends on factors such as  
529 satisfaction, perceived value, and personal involvement (Lai and Chen, 2011), the partnership  
530 established here with the public transit authority could increase the perceived value of public  
531 transit and increase ridership.

532 The repetitive nature of the TRAX transects gives insight into many processes that control  
533 the urban atmosphere and its linkages with human health and socioeconomic activities. The  
534 spatial extent of the TRAX rail network provides an excellent framework for these data to be  
535 used in combination with fixed observations sites to evaluate urban emission modeling and  
536 emission inventories of multiple species. Measurements of CO<sub>2</sub> could be used to monitor urban  
537 fossil fuel emissions and evaluate progress towards emission reduction targets such as Salt Lake  
538 City's goal of reducing greenhouse gas emissions by 50% in 2030 and 80% by 2040 compared to  
539 a baseline in 2009 (Salt Lake City Corporation, 2016). For CH<sub>4</sub>, examining and modeling the  
540 temporal signature of emissions from point sources could lead to new insight into the processes  
541 causing fugitive emissions (i.e. if they are associated with leaking infrastructure or if they are  
542 associated with operations). Integrating air quality observations from available sources could be

543 used to improve atmospheric models and estimates of pollutant exposure across urban areas and  
544 investigate the relationship with demographic characteristics and environmental justice issues.  
545 These observations and models could then be tied to spatially explicit human health impacts to  
546 improve our understanding of dose-response relationships at fine spatial scales across urban  
547 areas, which is relevant for public stakeholders and policymakers. These observations could also  
548 be used within a multi-species framework that leverages different emission patterns to reduce  
549 uncertainties in atmospheric transport, particularly during persistent cold air pools that are  
550 challenging to model and result in frequent violation of NAAQS. Also, the spatial footprint of  
551 the TRAX network (~25 km North-South and ~15 km East-West) may be suitable for ground-  
552 based evaluation of remote sensing instruments (i.e. satellite and aircraft) that are increasing their  
553 resolution to understand urban emissions and other processes with fine spatial variability. These  
554 data could also be used to compare and evaluate and calibrate high-density networks of low-cost  
555 instruments, such as the Purple Air network of low-cost air quality sensors (Kelly et al., 2017).  
556 Improving our understanding of urban GHG emissions and air pollutants will give policy makers  
557 vital information that will enable them to plan for how future urban growth will affect emissions  
558 and air quality. Finally, the real-time data can be used directly by the public to make informed  
559 decisions about their personal exposure to pollutants during their daily activities (e.g. recreation),  
560 and social scientists could study how access to spatially explicit real-time air quality information  
561 affects behavior.

562 While this initial study utilized only two light-rail train cars, it demonstrates the potential for  
563 leveraging public transit vehicles as a monitoring platform. This measurement strategy provides  
564 a cost-effective way to obtain spatial and temporal coverage across urban areas where GHG  
565 emissions and air quality health impacts are concentrated. Other modes of public transit (e.g.  
566 electric buses) could also be developed to expand this measurement strategy to other cities to  
567 better understand air quality across urban areas worldwide.

568

#### 569 **4. Acknowledgements**

570 The authors are grateful to the Utah Transit Authority (UTA) for supporting the installation  
571 of air quality sensors on their light rail trains. Special thanks go to James (Tal) Brooks, Teresa  
572 Jessen, Dan Christenson, William Patterson, and Elijah Jackson at UTA for assistance with the  
573 equipment installation and ongoing access to the trains for maintenance. We also thank the

574 Center for High Performance Computing at the University of Utah for their support and  
575 resources, Google Earth for data visualization, Maria Garcia for calibration tanks, Ryan Bares  
576 and the DAQ for providing stationary site measurements for comparisons, LGR for loaning us  
577 their NO<sub>2</sub> analyzer, Munkhbayar Baasandorj, the DAQ, and the NOAA ESRL Twin Otter  
578 aircraft group for assistance with calibration of the NO<sub>2</sub> analyzer, and two anonymous reviewers  
579 who provided constructive feedback that improved the manuscript. This work was partially  
580 supported by grants from the Utah DAQ (150697), NSF (EF-1137336, OAC-1443046), NOAA  
581 (NA14OAR4310178) and DOE (DE-SC0010625).

582 **5. Tables**

**Table 1**

Measurement equipment deployed on TRAX train cars.

Instrument	Species	Sample rate	Measurement uncertainty	TRAX Train car
Met One Instruments E-Sampler	PM <sub>2.5</sub>	1 min.	1 µg m <sup>-3</sup>	1
Met One Instruments ES-642 Remote Dust Monitor	PM <sub>2.5</sub>	1 sec.	1 µg m <sup>-3</sup>	2
2B Technologies Model 205 Ozone Monitor	O <sub>3</sub>	2 sec.	2%	1 and 2
Los Gatos Research Ultra-portable Greenhouse Gas Analyzer	CO <sub>2</sub>	1 sec.	0.3 ppm CO <sub>2</sub>	1
	CH <sub>4</sub>		2 ppb CH <sub>4</sub>	
	H <sub>2</sub> O		100 ppm H <sub>2</sub> O	
Los Gatos Research NO <sub>2</sub> Analyzer	NO <sub>2</sub>	1 sec.	0.05 ppb	2

583

584

585 **6. Figures**

586

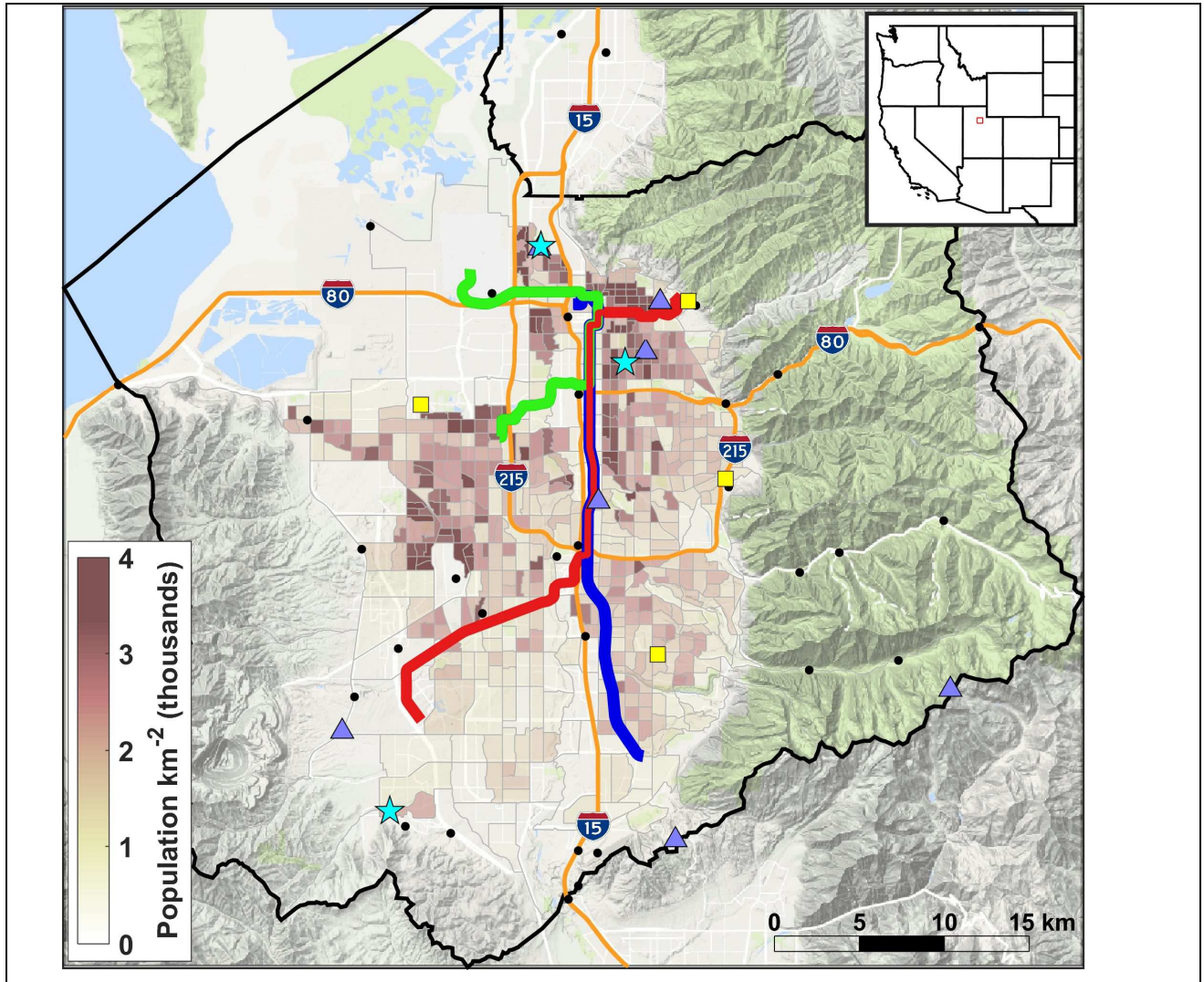


Figure 1. The TRAX Red, Green, and Blue train lines in the Salt Lake Valley (SLV). The University of Utah greenhouse gas monitoring network (blue triangles), research grade air quality stations (yellow squares), surface weather stations courtesy of MesoWest (black dots (Horel et al., 2002)), and the Utah Division of Air Quality’s Hawthorne site (cyan star 2 km east of where the Green and Red lines overlap) are also shown. The population density is superimposed in brown shading, and the inset shows the location of the SLV as a red box in the western U.S.

587

588

589

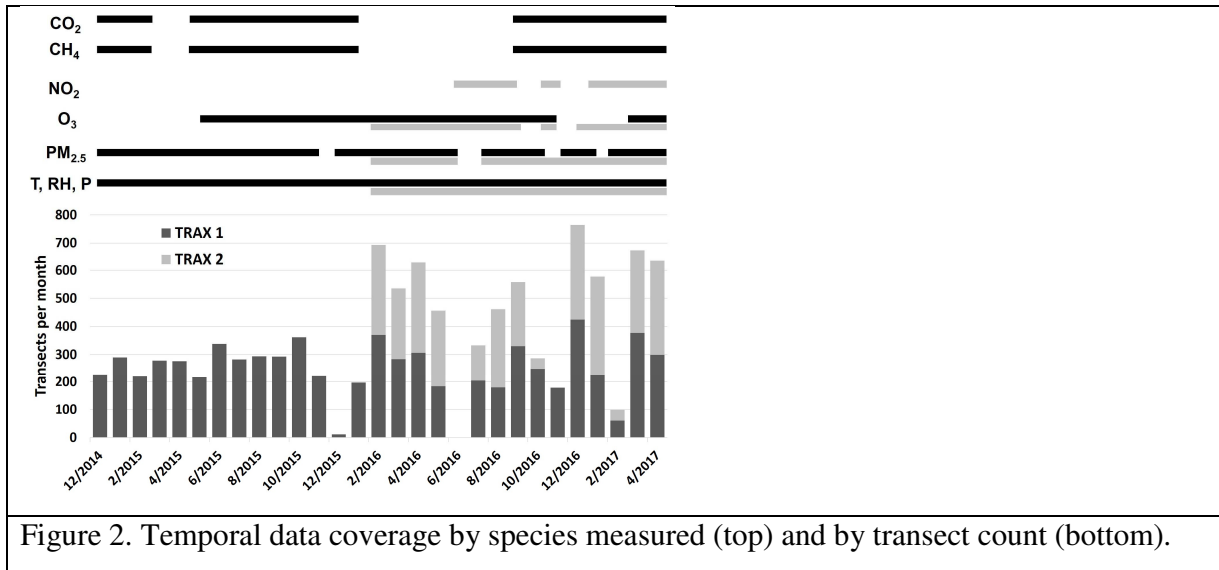


Figure 2. Temporal data coverage by species measured (top) and by transect count (bottom).

590

591

592

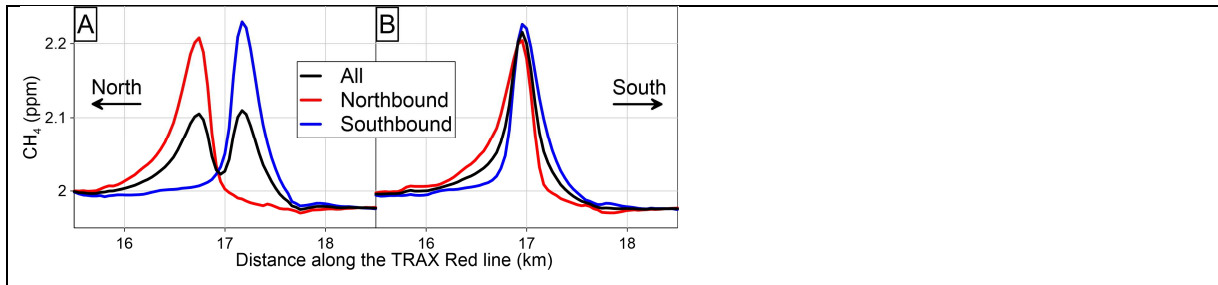


Figure 3. Example of an empirical determination of the time lag due to the amount of time it takes for a parcel of air to travel the length of the inlet tubing to the instrument. In the raw data, without a lag time applied to the data, a persistent feature in the CH<sub>4</sub> measurements along the Red TRAX line was shifted north (south) of the central location when the train was traveling northbound (southbound) (A). When a time lag was applied to the data (in this case a 9-second lag) the peak occurred in the same location when the northbound and southbound data were averaged (B).

593

594

595



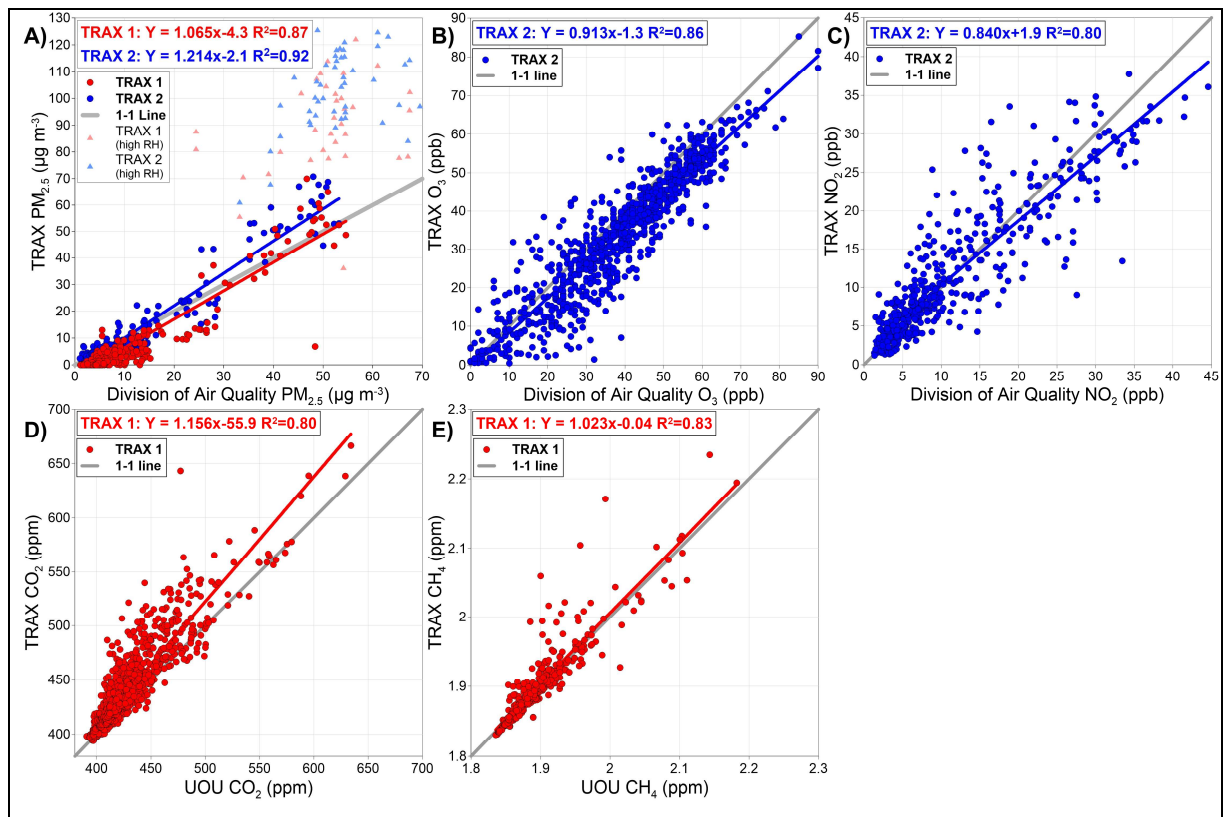


Figure 4. Comparisons of TRAX measurements against measurements made at stationary sites. The top row (panels A-C) shows comparisons of air pollutants PM<sub>2.5</sub>, O<sub>3</sub>, and NO<sub>2</sub> against the Utah Division of Air Quality Hawthorne site (cyan star in Figure 1) while the bottom row (panels D and E) shows comparisons of greenhouse gases CO<sub>2</sub> and CH<sub>4</sub> against the UOU site (the northeastern most blue triangle adjacent to the Red line in Figure 1).

597

598

599

600

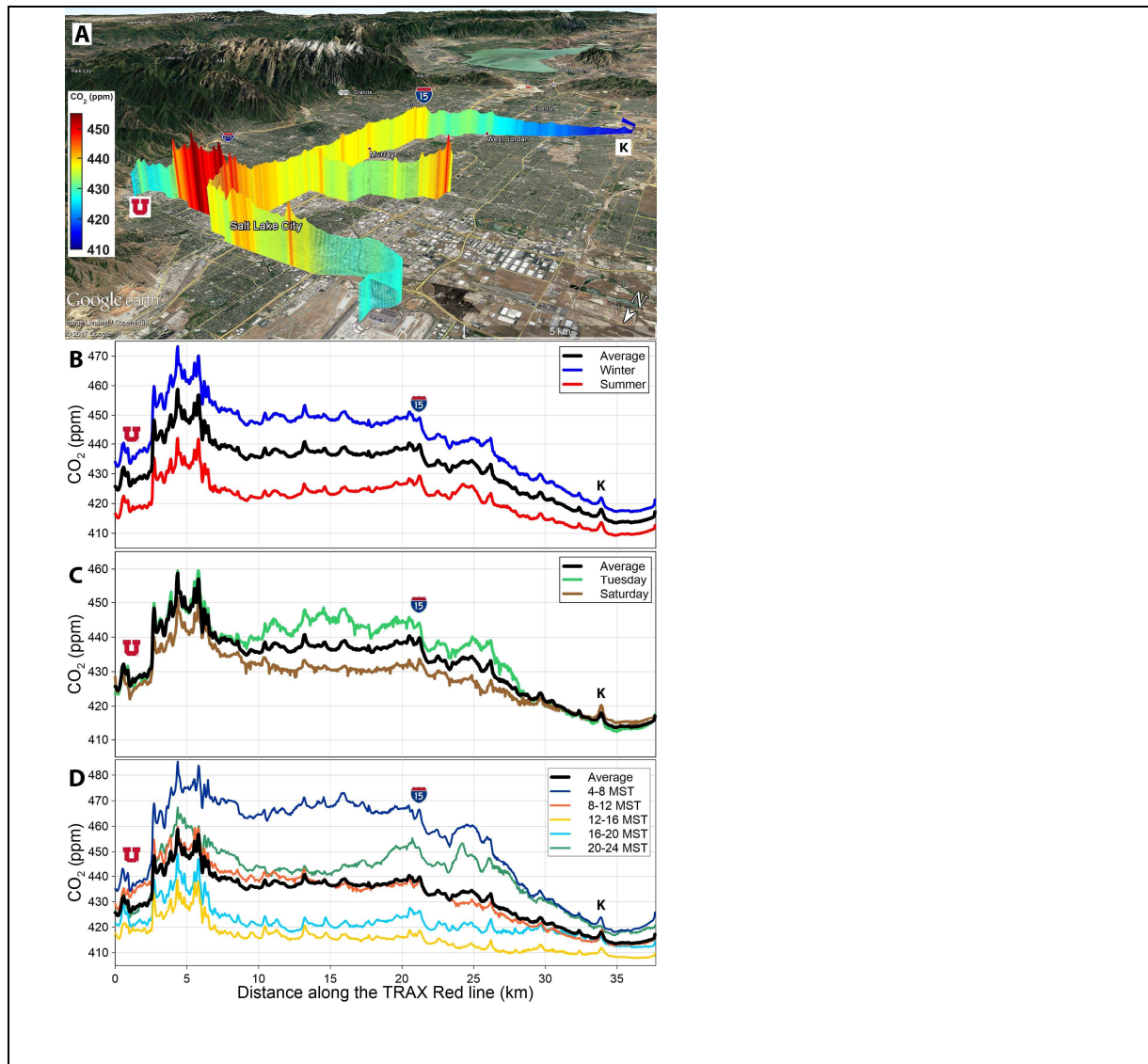


Figure 5. Spatially and temporally averaged carbon dioxide (CO<sub>2</sub>) in the SLV between December 2014 and April 2017 along the Red and Green TRAX train lines (A). The lower panels show seasonal (B), day of week (C), and diel (D) averages, as compared to the overall average that is shown in panel A (the overall average is indicated by the black line in panels B-D). Winter (summer) months were averaged over October-March (April-August). The location of the University of Utah and the UOU stationary measurement site on the northeastern foothills of the SLV is indicated with a red 'U'. Also, the location where the Red line crosses the I-15 interstate freeway, and where it passes next to a brick factory are indicated with an I-15 placard and a 'K', respectively.

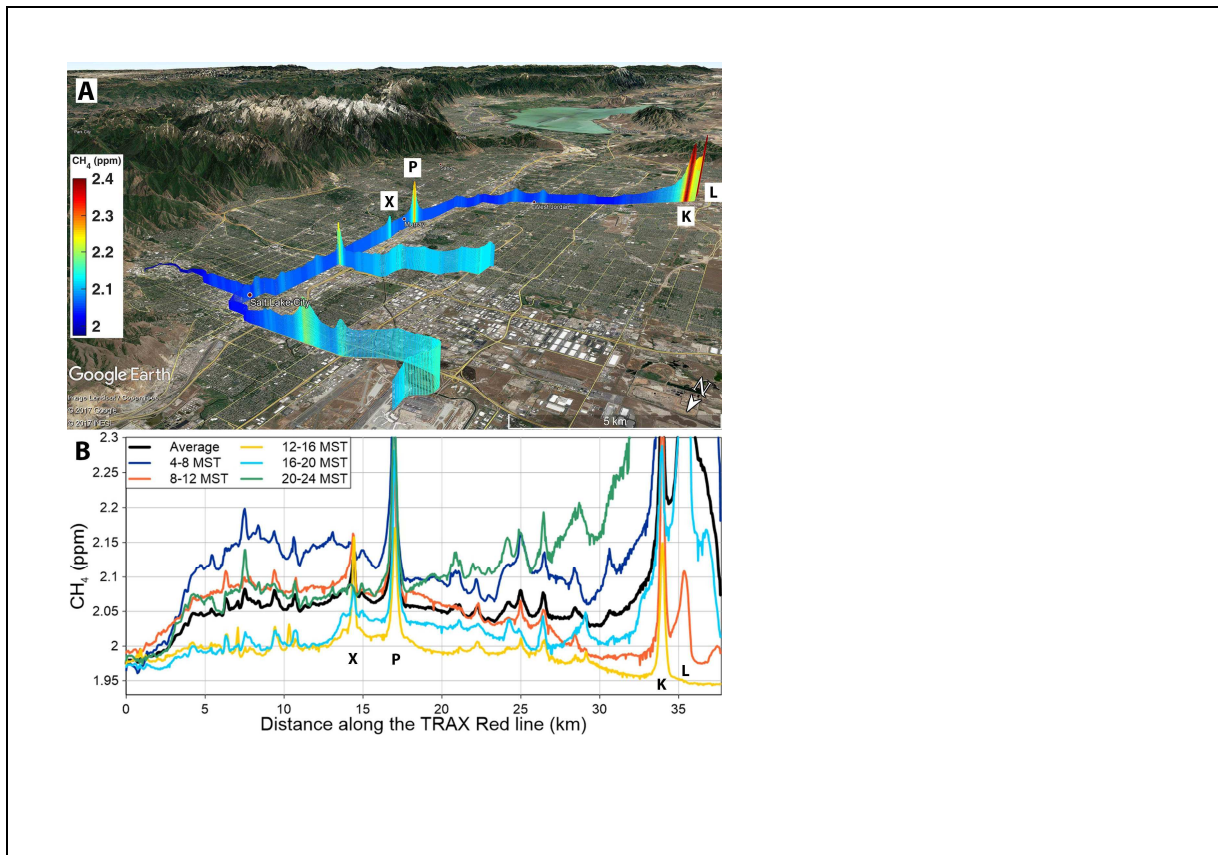
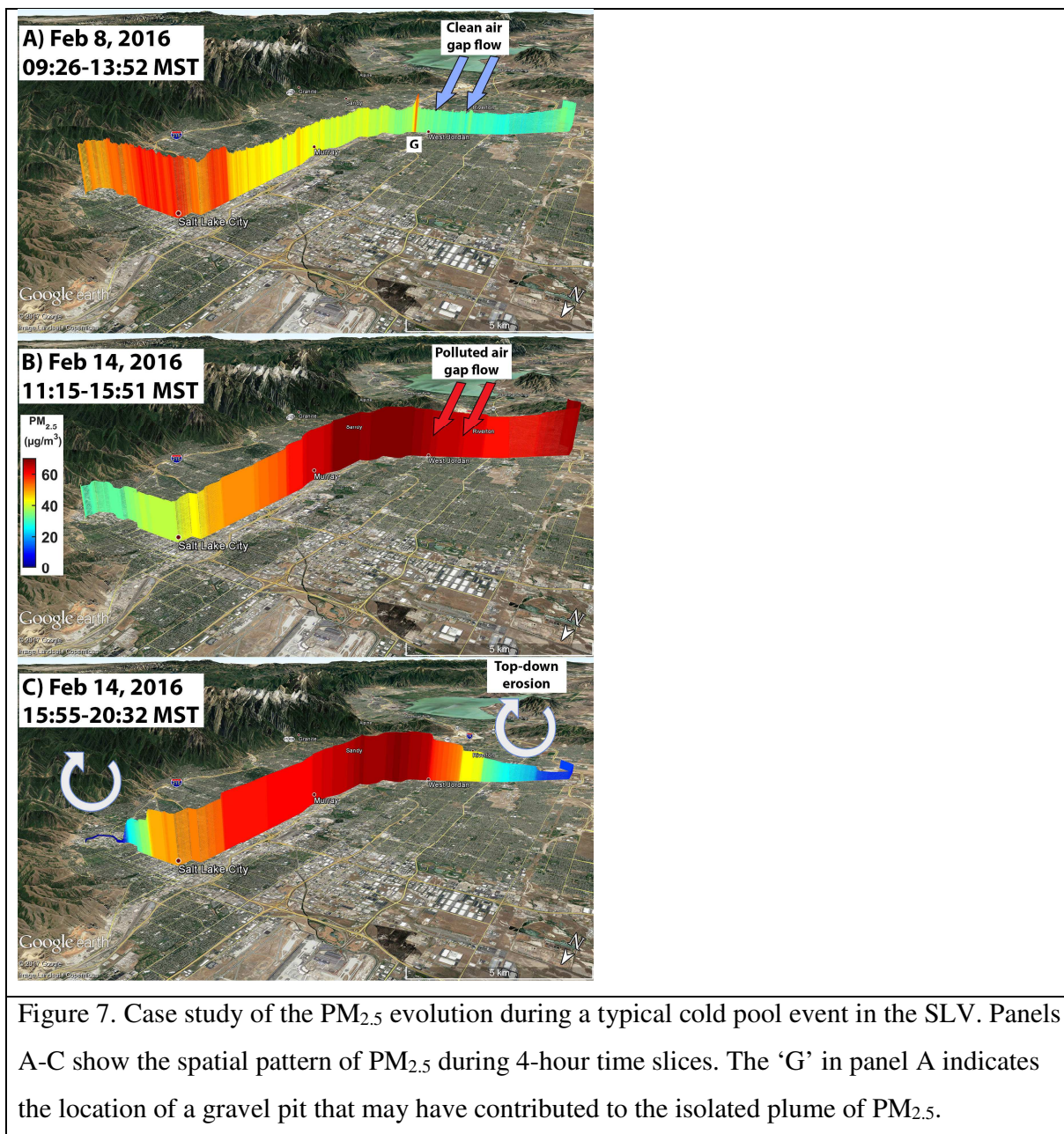


Figure 6. Spatially and temporally averaged methane ( $\text{CH}_4$ ) in the SLV between December 2014 and April 2017 (A) and average concentrations during 4-hour time windows along the Red line (B). The overall average (black line) in B is the same as the Red train line data shown in A. The letters in both panels indicate the locations of an intermittent plume from an unknown source (X), a natural gas power plant (P), a brick factory that uses a natural gas fired kiln (K), and a landfill (L).



606

607

608

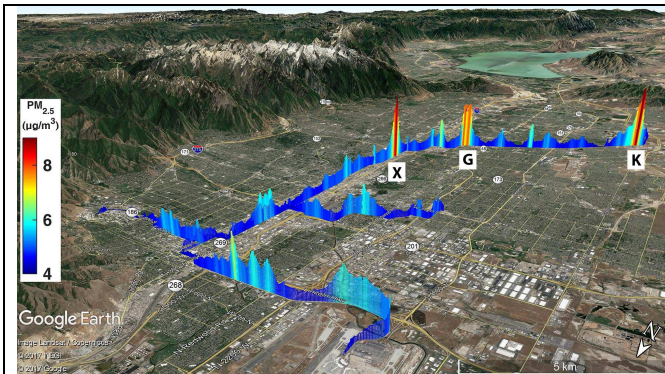


Figure 8. PM<sub>2.5</sub> averaged over the summer of 2016 (May through September). The ‘G’, ‘K’, and ‘X’ indicate the locations of the gravel pit shown in Figure 7a, the brick factory shown in Figure 5 and Figure 6, and an unidentified PM<sub>2.5</sub> source, respectively.

609

610

611

612

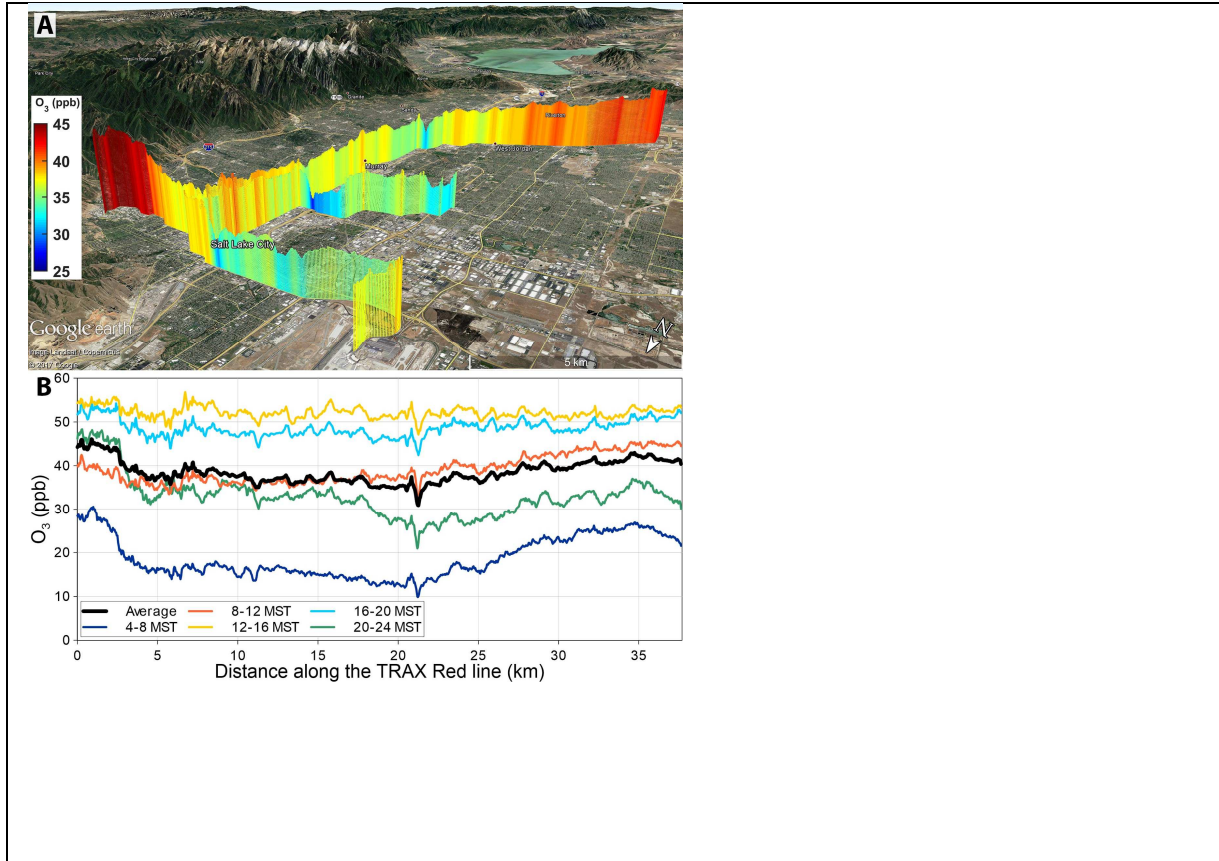


Figure 9. The ozone ( $O_3$ ) average during the summer season from May to September 2015 in the SLV (A) and average concentrations during 4-hour time windows along the Red train line (B). The overall average (black line) in B is the same as the Red line data shown in A.

613

614

615

616

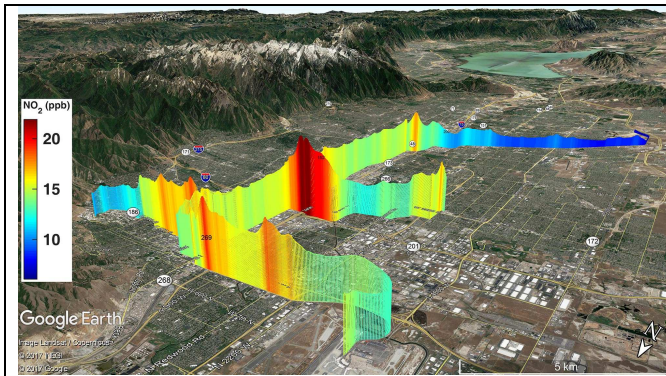


Figure 10. The nitrogen dioxide ( $\text{NO}_2$ ) average over one year from June 2016 to June 2017.

617

618

619

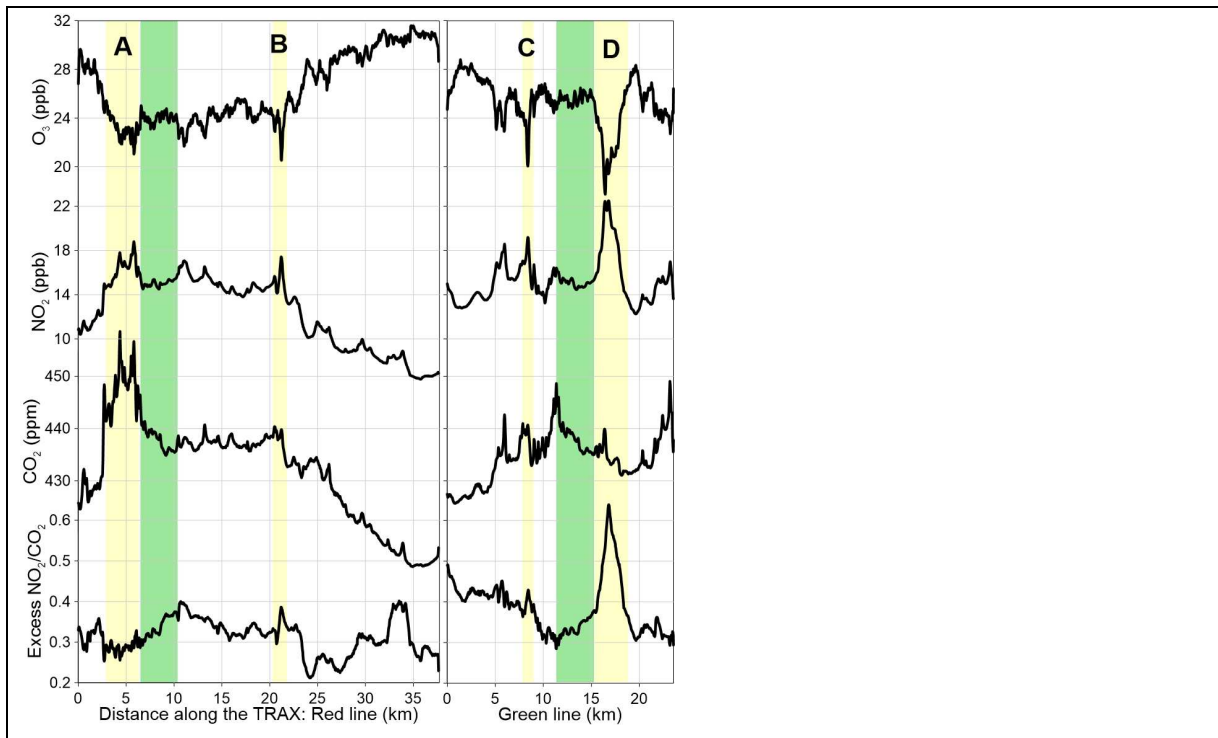


Figure 11. Temporally averaged  $O_3$ ,  $NO_2$ ,  $CO_2$  and the excess  $NO_2/CO_2$  ratio along both of the TRAX lines.  $O_3$  and  $NO_2$  were measured on TRAX 2 while  $CO_2$  was measured on TRAX 1, however since they consist of >1 year of data, the averages can be compared to each other. The yellow shaded areas indicate where the TRAX line is in the middle of a roadway near downtown (A), and crosses I-15 on the Red line (B) and on the Green line (C and D). The green shading indicates where the Red and Green train lines overlap each other.



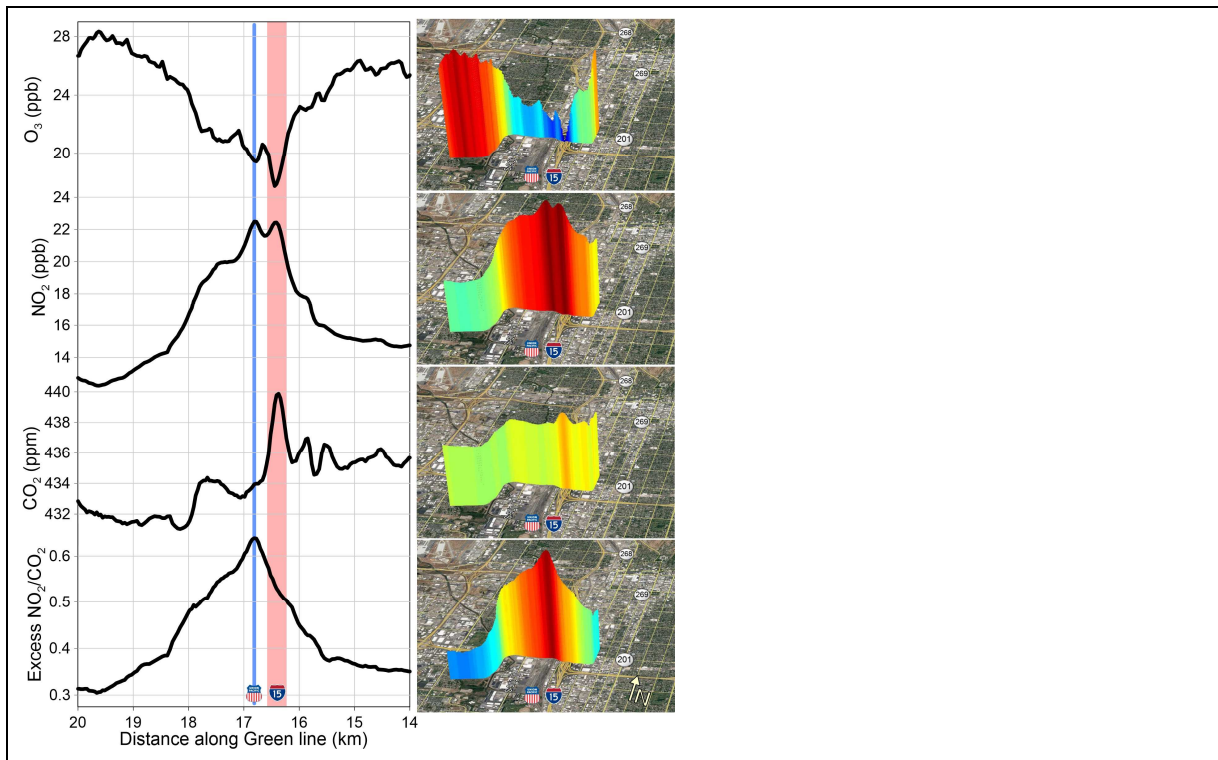


Figure 12. Relationships between species illustrating sources of  $\text{NO}_2$  and  $\text{CO}_2$  along a subsection of the Green line. The Union Pacific rail yard and I-15 interstate highway are indicated with a blue line and red shading respectively in the left panel and with icons in both the left and right panels. The scale in the left panels corresponds to the shading in the right panels. Note that these Google Earth images are looking northwest to see the Union Pacific rail yard that is just south of the TRAX rail line, whereas the prior Google Earth images were looking southeast.

624

625

626

627

628

## 629 7. References

630

631 References that have been accepted for publication:

632 John Lin, Logan Mitchell, Erik Crosman, Daniel Mendoza, Martin Buchert, Ryan Bares, Ben  
633 Fasoli, Dave Bowling, Diane Pataki, Doug Catharine, Courtenay Strong, Kevin Gurney,  
634 Risa Patarasuk, Munkhbayar Baasandorj, Alex Jacques, Sebastian Hoch, Jim Ehleringer  
635 (*in press at BAMS*), CO<sub>2</sub> and carbon emissions from cities: linkages to air quality,  
636 socioeconomic activity and stakeholders in the Salt Lake City urban area

637

638 Published references:

639

640 Air Quality Research Subcommittee, 2013. Air Quality Observation Systems in the United  
641 States. Committee on Environment, Natural Resources, and Sustainability.

642 Apte, J.S., Messier, K.P., Gani, S., Brauer, M., Kirchstetter, T.W., Lunden, M.M., Marshall, J.D.,  
643 Portier, C.J., Vermeulen, R.C.H., Hamburg, S.P., 2017. High-Resolution Air Pollution  
644 Mapping with Google Street View Cars: Exploiting Big Data. *Environ. Sci. Technol.* 51,  
645 6999–7008. <https://doi.org/10.1021/acs.est.7b00891>

646 Baasandorj, M., Hoch, S.W., Bares, R., Lin, J.C., Brown, S.S., Millet, D.B., Martin, R., Kelly,  
647 K., Zarzana, K.J., Whiteman, C.D., Dube, W.P., Tonnesen, G., Jaramillo, I.C., Sohl, J.,  
648 2017. Coupling between Chemical and Meteorological Processes under Persistent Cold-  
649 Air Pool Conditions: Evolution of Wintertime PM<sub>2.5</sub> Pollution Events and N<sub>2</sub>O<sub>5</sub>  
650 Observations in Utah's Salt Lake Valley. *Environ. Sci. Technol.* 51, 5941–5950.  
651 <https://doi.org/10.1021/acs.est.6b06603>

652 Baldauf, R., Thoma, E., Hays, M., Shores, R., Kinsey, J., Gullett, B., Kimbrough, S., Isakov, V.,  
653 Long, T., Snow, R., Khlystov, A., Weinstein, J., Chen, F.-L., Seila, R., Olson, D.,  
654 Gilmour, I., Cho, S.-H., Watkins, N., Rowley, P., Bang, J., 2008. Traffic and  
655 Meteorological Impacts on Near-Road Air Quality: Summary of Methods and Trends  
656 from the Raleigh Near-Road Study. *J. Air Waste Manag. Assoc.* 58, 865–878.  
657 <https://doi.org/10.3155/1047-3289.58.7.865>

658 Barakeh, Z.A., Breuil, P., Redon, N., Pijolat, C., Locoge, N., Viricelle, J.-P., 2017. Development  
659 of a normalized multi-sensors system for low cost on-line atmospheric pollution  
660 detection. *Sens. Actuators B Chem.* 241, 1235–1243.  
661 <https://doi.org/10.1016/j.snb.2016.10.006>

662 Bares, R., Lin John C., Hoch Sebastian W., Baasandorj Munkhbayar, Mendoza Daniel L., Fasoli  
663 Ben, Mitchell Logan, Catharine Douglas, Stephens Britton B., 2018. The Wintertime  
664 Covariation of CO<sub>2</sub> and Criteria Pollutants in an Urban Valley of the Western United  
665 States. *J. Geophys. Res. Atmospheres* 0. <https://doi.org/10.1002/2017JD027917>

666 Bateman, M., Collard, C., Teigen, S., 2016. Part I: Survey of Voters' Issues and Concerns (No.  
667 739), 2016 Utah Priorities Project. Utah Foundation.

- 668 Blaylock, B., Horel, J.D., Crosman, E.T., 2016. Impact of Lake Breezes on Summer Ozone  
669 Concentrations in the Salt Lake Valley. *J. Appl. Meteorol. Climatol.* 56, 353–370.  
670 <https://doi.org/10.1175/JAMC-D-16-0216.1>
- 671 Borrego, C., Costa, A.M., Ginja, J., Amorim, M., Coutinho, M., Karatzas, K., Sioumis, T.,  
672 Katsifarakis, N., Konstantinidis, K., De Vito, S., Esposito, E., Smith, P., André, N.,  
673 Gérard, P., Francis, L.A., Castell, N., Schneider, P., Viana, M., Minguillón, M.C.,  
674 Reimringer, W., Otjes, R.P., von Sicard, O., Pohle, R., Elen, B., Suriano, D., Pfister, V.,  
675 Prato, M., Dipinto, S., Penza, M., 2016. Assessment of air quality microsensors versus  
676 reference methods: The EuNetAir joint exercise. *Atmos. Environ.* 147, 246–263.  
677 <https://doi.org/10.1016/j.atmosenv.2016.09.050>
- 678 Brent, L.C., Thorn, W.J., Gupta, M., Leen, B., Stehr, J.W., He, H., Arkinson, H.L., Weinheimer,  
679 A., Garland, C., Pusede, S.E., Wooldridge, P.J., Cohen, R.C., Dickerson, R.R., 2013.  
680 Evaluation of the use of a commercially available cavity ringdown absorption  
681 spectrometer for measuring NO<sub>2</sub> in flight, and observations over the Mid-Atlantic States,  
682 during DISCOVER-AQ. *J. Atmospheric Chem.* 72, 503–521.  
683 <https://doi.org/10.1007/s10874-013-9265-6>
- 684 Brunekreef, B., Holgate, S.T., 2002. Air pollution and health. *The Lancet* 360, 1233–1242.  
685 [https://doi.org/10.1016/S0140-6736\(02\)11274-8](https://doi.org/10.1016/S0140-6736(02)11274-8)
- 686 Castell, N., Kobernus, M., Liu, H.-Y., Schneider, P., Lahoz, W., Berre, A.J., Noll, J., 2015.  
687 Mobile technologies and services for environmental monitoring: The Citi-Sense-MOB  
688 approach. *Urban Clim., New Sensing Technologies and Methods for Air Pollution*  
689 *Monitoring* 14, Part 3, 370–382. <https://doi.org/10.1016/j.uclim.2014.08.002>
- 690 Castellini, S., Moroni, B., Cappelletti, D., 2014. PMetro: Measurement of urban aerosols on a  
691 mobile platform. *Measurement* 49, 99–106.  
692 <https://doi.org/10.1016/j.measurement.2013.11.045>
- 693 Chen, H., Kwong, J.C., Copes, R., Tu, K., Villeneuve, P.J., Donkelaar, A. van, Hystad, P.,  
694 Martin, R.V., Murray, B.J., Jessiman, B., Wilton, A.S., Kopp, A., Burnett, R.T., 2017.  
695 Living near major roads and the incidence of dementia, Parkinson’s disease, and multiple  
696 sclerosis: a population-based cohort study. *The Lancet* 389, 718–726.  
697 [https://doi.org/10.1016/S0140-6736\(16\)32399-6](https://doi.org/10.1016/S0140-6736(16)32399-6)
- 698 Christen, A., Coops, N.C., Crawford, B.R., Kellett, R., Liss, K.N., Olchovski, I., Tooke, T.R.,  
699 van der Laan, M., Voogt, J.A., 2011. Validation of modeled carbon-dioxide emissions  
700 from an urban neighborhood with direct eddy-covariance measurements. *Atmos. Environ.*  
701 45, 6057–6069. <https://doi.org/10.1016/j.atmosenv.2011.07.040>
- 702 Clements, A.L., Griswold, W.G., Rs, A., Johnston, J.E., Herting, M.M., Thorson, J., Collier-  
703 Oxandale, A., Hannigan, M., 2017. Low-Cost Air Quality Monitoring Tools: From  
704 Research to Practice (A Workshop Summary). *Sensors* 17, 2478.  
705 <https://doi.org/10.3390/s17112478>
- 706 Correia, A.W., Pope, C.A., Dockery, D.W., Wang, Y., Ezzati, M., Dominici, F., 2013. The Effect  
707 of Air Pollution Control on Life Expectancy in the United States: An Analysis of 545 US  
708 counties for the period 2000 to 2007. *Epidemiol. Camb. Mass* 24, 23–31.  
709 <https://doi.org/10.1097/EDE.0b013e3182770237>
- 710 Crosman, E.T., Horel, J.D., 2016. Winter Lake Breezes near the Great Salt Lake. *Bound.-Layer*  
711 *Meteorol.* 159, 439–464. <https://doi.org/10.1007/s10546-015-0117-6>

712 Crosman, E.T., Jacques, A.A., Horel, J.D., 2017. A novel approach for monitoring vertical  
713 profiles of boundary-layer pollutants: Utilizing routine news helicopter flights.  
714 *Atmospheric Pollut. Res.* 8, 828–835. <https://doi.org/10.1016/j.apr.2017.01.013>

715 Deville Cavellin, L., Weichenthal, S., Tack, R., Ragetti, M.S., Smargiassi, A., Hatzopoulou, M.,  
716 2016. Investigating the Use Of Portable Air Pollution Sensors to Capture the Spatial  
717 Variability Of Traffic-Related Air Pollution. *Environ. Sci. Technol.* 50, 313–320.  
718 <https://doi.org/10.1021/acs.est.5b04235>

719 Di, Q., Wang, Yan, Zanobetti, A., Wang, Yun, Koutrakis, P., Choirat, C., Dominici, F.,  
720 Schwartz, J.D., 2017. Air Pollution and Mortality in the Medicare Population. *N. Engl. J.*  
721 *Med.* 376, 2513–2522. <https://doi.org/10.1056/NEJMoa1702747>

722 Dlugokencky, E.J., Myers, R.C., Lang, P.M., Masarie, K.A., Crotwell, A.M., Thoning, K.W.,  
723 Hall, B.D., Elkins, J.W., Steele, L.P., 2005. Conversion of NOAA atmospheric dry air  
724 CH<sub>4</sub> mole fractions to a gravimetrically prepared standard scale. *J. Geophys. Res.-*  
725 *Atmospheres* 110, 8.

726 Franklin, M., Zeka, A., Schwartz, J., 2006. Association between PM<sub>2.5</sub> and all-cause and  
727 specific-cause mortality in 27 US communities. *J. Expo. Sci. Environ. Epidemiol.* 17,  
728 279–287. <https://doi.org/10.1038/sj.jes.7500530>

729 Gozzi, F., Della Ventura, G., Marcelli, A., 2016. Mobile monitoring of particulate matter: State  
730 of art and perspectives. *Atmospheric Pollut. Res.* 7, 228–234.  
731 <https://doi.org/10.1016/j.apr.2015.09.007>

732 Gurney, K.R., Mendoza, D.L., Zhou, Y., Fischer, M.L., Miller, C.C., Geethakumar, S., de la Rue  
733 du Can, S., 2009. High Resolution Fossil Fuel Combustion CO<sub>2</sub> Emission Fluxes for the  
734 United States. *Environ. Sci. Technol.* 43, 5535–5541. <https://doi.org/10.1021/es900806c>

735 Gurney, K.R., Romero-Lankao, P., Seto, K.C., Hutyra, L.R., Duren, R., Kennedy, C., Grimm,  
736 N.B., Ehleringer, J.R., Marcotullio, P., Hughes, S., Pincetl, S., Chester, M.V., Runfola,  
737 D.M., Feddema, J.J., Sperling, J., 2015. Climate change: Track urban emissions on a  
738 human scale. *Nature* 525, 179–181. <https://doi.org/10.1038/525179a>

739 Hagemann, R., Corsmeier, U., Kottmeier, C., Rinke, R., Wieser, A., Vogel, B., 2014. Spatial  
740 variability of particle number concentrations and NO<sub>x</sub> in the Karlsruhe (Germany) area  
741 obtained with the mobile laboratory ‘AERO-TRAM.’ *Atmos. Environ.* 94, 341–352.  
742 <https://doi.org/10.1016/j.atmosenv.2014.05.051>

743 Hasenfratz, D., Saukh, O., Walser, C., Hueglin, C., Fierz, M., Arn, T., Beutel, J., Thiele, L.,  
744 2015. Deriving high-resolution urban air pollution maps using mobile sensor nodes.  
745 *Pervasive Mob. Comput., Selected Papers from the Twelfth Annual IEEE International*  
746 *Conference on Pervasive Computing and Communications (PerCom 2014)* 16, Part B,  
747 268–285. <https://doi.org/10.1016/j.pmcj.2014.11.008>

748 Hoek, G., Beelen, R., de Hoogh, K., Vienneau, D., Gulliver, J., Fischer, P., Briggs, D., 2008. A  
749 review of land-use regression models to assess spatial variation of outdoor air pollution.  
750 *Atmos. Environ.* 42, 7561–7578. <https://doi.org/10.1016/j.atmosenv.2008.05.057>

751 Hopkins, F.M., Kort, E.A., Bush, S.E., Ehleringer, J.R., Lai, C.-T., Blake, D.R., Randerson, J.T.,  
752 2016. Spatial patterns and source attribution of urban methane in the Los Angeles Basin.  
753 *J. Geophys. Res. Atmospheres* 121, 2015JD024429.  
754 <https://doi.org/10.1002/2015JD024429>

755 Horel, J., Crosman, E., Jacques, A., Blaylock, B., Arens, S., Long, A., Sohl, J., Martin, R., 2016.  
756 Summer ozone concentrations in the vicinity of the Great Salt Lake. *Atmospheric Sci.*  
757 *Lett.* 17, 480–486. <https://doi.org/10.1002/asl.680>

758 Horel, J., Splitt, M., Dunn, L., Pechmann, J., White, B., Ciliberti, C., Lazarus, S., Slemmer, J.,  
759 Zaff, D., Burks, J., 2002. Mesowest: Cooperative mesonets in the western United States.  
760 Bull. Am. Meteorol. Soc. 83, 211–225.

761 Hutyra, L.R., Duren, R., Gurney, K.R., Grimm, N., Kort, E.A., Larson, E., Shrestha, G., 2014.  
762 Urbanization and the carbon cycle: Current capabilities and research outlook from the  
763 natural sciences perspective. *Earths Future* 2, 473–495.  
764 <https://doi.org/10.1002/2014EF000255>

765 Idso, C.D., Idso, S.B., Balling Jr., R.C., 2001. An intensive two-week study of an urban CO<sub>2</sub>  
766 dome in Phoenix, Arizona, USA. *Atmos. Environ.* 35, 995–1000.  
767 [https://doi.org/10.1016/S1352-2310\(00\)00412-X](https://doi.org/10.1016/S1352-2310(00)00412-X)

768 Jackson, R.B., Down, A., Phillips, N.G., Ackley, R.C., Cook, C.W., Plata, D.L., Zhao, K., 2014.  
769 Natural Gas Pipeline Leaks Across Washington, DC. *Environ. Sci. Technol.* 48, 2051–  
770 2058. <https://doi.org/10.1021/es404474x>

771 Jiao, W., Hagler, G., Williams, R., Sharpe, R., Brown, R., Garver, D., Judge, R., Caudill, M.,  
772 Rickard, J., Davis, M., Weinstock, L., Zimmer-Dauphinee, S., Buckley, K., 2016.  
773 Community Air Sensor Network (CAIRSENSE) project: evaluation of low-cost sensor  
774 performance in a suburban environment in the southeastern United States. *Atmos Meas*  
775 *Tech* 9, 5281–5292. <https://doi.org/10.5194/amt-9-5281-2016>

776 Jung, S., Lee, M., Kim, J., Lyu, Y., Park, J., 2011. Speed-dependent emission of air pollutants  
777 from gasoline-powered passenger cars. *Environ. Technol.* 32, 1173–1181.  
778 <https://doi.org/10.1080/09593330.2010.505611>

779 Kelly, K.E., Whitaker, J., Petty, A., Widmer, C., Dybwad, A., Sleeth, D., Martin, R., Butterfield,  
780 A., 2017. Ambient and laboratory evaluation of a low-cost particulate matter sensor.  
781 *Environ. Pollut.* 221, 491–500. <https://doi.org/10.1016/j.envpol.2016.12.039>

782 Kumar, P., Morawska, L., Martani, C., Biskos, G., Neophytou, M., Di Sabatino, S., Bell, M.,  
783 Norford, L., Britter, R., 2015. The rise of low-cost sensing for managing air pollution in  
784 cities. *Environ. Int.* 75, 199–205. <https://doi.org/10.1016/j.envint.2014.11.019>

785 Lai, W.-T., Chen, C.-F., 2011. Behavioral intentions of public transit passengers—The roles of  
786 service quality, perceived value, satisfaction and involvement. *Transp. Policy* 18, 318–  
787 325. <https://doi.org/10.1016/j.tranpol.2010.09.003>

788 Lamb, B.K., Cambaliza, M.O.L., Davis, K.J., Edburg, S.L., Ferrara, T.W., Floerchinger, C.,  
789 Heimbürger, A.M.F., Herndon, S., Lauvaux, T., Lavoie, T., Lyon, D.R., Miles, N.,  
790 Prasad, K.R., Richardson, S., Roscioli, J.R., Salmon, O.E., Shepson, P.B., Stirm, B.H.,  
791 Whetstone, J., 2016. Direct and Indirect Measurements and Modeling of Methane  
792 Emissions in Indianapolis, Indiana. *Environ. Sci. Technol.* 50, 8910–8917.  
793 <https://doi.org/10.1021/acs.est.6b01198>

794 Landrigan, P.J., Fuller, R., Acosta, N.J.R., Adeyi, O., Arnold, R., Basu, N. (Nil), Baldé, A.B.,  
795 Bertollini, R., Bose-O'Reilly, S., Boufford, J.I., Breysse, P.N., Chiles, T., Mahidol, C.,  
796 Coll-Seck, A.M., Cropper, M.L., Fobil, J., Fuster, V., Greenstone, M., Haines, A.,  
797 Hanrahan, D., Hunter, D., Khare, M., Krupnick, A., Lanphear, B., Lohani, B., Martin, K.,  
798 Mathiasen, K.V., McTeer, M.A., Murray, C.J.L., Ndahimananjara, J.D., Perera, F.,  
799 Potočník, J., Preker, A.S., Ramesh, J., Rockström, J., Salinas, C., Samson, L.D.,  
800 Sandilya, K., Sly, P.D., Smith, K.R., Steiner, A., Stewart, R.B., Suk, W.A., Schayck,  
801 O.C.P. van, Yadama, G.N., Yumkella, K., Zhong, M., 2017. The Lancet Commission on  
802 pollution and health. *The Lancet* 0. [https://doi.org/10.1016/S0140-6736\(17\)32345-0](https://doi.org/10.1016/S0140-6736(17)32345-0)

803 Lareau, N.P., Horel, J.D., 2015. Dynamically Induced Displacements of a Persistent Cold-Air  
804 Pool. *Bound.-Layer Meteorol.* 154, 291–316. <https://doi.org/10.1007/s10546-014-9968-5>

805 Lareau, N.P., Horel, J.D., 2014. Turbulent Erosion of Persistent Cold-Air Pools: Numerical  
806 Simulations. *J. Atmospheric Sci.* 72, 1409–1427. <https://doi.org/10.1175/JAS-D-14-0173.1>

807

808 Le Quéré, C., Andrew, R.M., Canadell, J.G., Sitch, S., Korsbakken, J.I., Peters, G.P., Manning,  
809 A.C., Boden, T.A., Tans, P.P., Houghton, R.A., Keeling, R.F., Alin, S., Andrews, O.D.,  
810 Anthoni, P., Barbero, L., Bopp, L., Chevallier, F., Chini, L.P., Ciais, P., Currie, K.,  
811 Delire, C., Doney, S.C., Friedlingstein, P., Gkritzalis, T., Harris, I., Hauck, J., Haverd, V.,  
812 Hoppema, M., Klein Goldewijk, K., Jain, A.K., Kato, E., Körtzinger, A., Landschützer,  
813 P., Lefèvre, N., Lenton, A., Lienert, S., Lombardozzi, D., Melton, J.R., Metzl, N.,  
814 Millero, F., Monteiro, P.M.S., Munro, D.R., Nabel, J.E.M.S., Nakaoka, S., O'Brien, K.,  
815 Olsen, A., Omar, A.M., Ono, T., Pierrot, D., Poulter, B., Rödenbeck, C., Salisbury, J.,  
816 Schuster, U., Schwinger, J., Séférian, R., Skjelvan, I., Stocker, B.D., Sutton, A.J.,  
817 Takahashi, T., Tian, H., Tilbrook, B., Laan-Luijkx, I.T. van der, Werf, G.R. van der,  
818 Viovy, N., Walker, A.P., Wiltshire, A.J., Zaehle, S., 2016. Global Carbon Budget 2016.  
819 *Earth Syst. Sci. Data* 8, 605–649. <https://doi.org/10.5194/essd-8-605-2016>

820 Lee, J.K., Christen, A., Ketler, R., Nesic, Z., 2017. A mobile sensor network to map carbon  
821 dioxide emissions in urban environments. *Atmos Meas Tech* 10, 645–665.  
822 <https://doi.org/10.5194/amt-10-645-2017>

823 Mallia, D.V., Kochanski, A., Wu, D., Pennell, C., Oswald, W., Lin, J.C., 2017. Wind-Blown  
824 Dust Modeling Using a Backward-Lagrangian Particle Dispersion Model. *J. Appl.*  
825 *Meteorol. Climatol.* 56, 2845–2867. <https://doi.org/10.1175/JAMC-D-16-0351.1>

826 Mallia, D.V., Lin, J.C., Urbanski, S., Ehleringer, J., Nehr Korn, T., 2015. Impacts of upwind  
827 wildfire emissions on CO, CO<sub>2</sub>, and PM<sub>2.5</sub> concentrations in Salt Lake City, Utah. *J.*  
828 *Geophys. Res. Atmospheres* 120, 2014JD022472. <https://doi.org/10.1002/2014JD022472>

829 Matte, T.D., Ross, Z., Kheirbek, I., Eisl, H., Johnson, S., Gorczynski, J.E., Kass, D., Markowitz,  
830 S., Pezeshki, G., Clougherty, J.E., 2013. Monitoring intraurban spatial patterns of  
831 multiple combustion air pollutants in New York City: Design and implementation. *J.*  
832 *Expo. Sci. Environ. Epidemiol.* 23, 223–231. <https://doi.org/10.1038/jes.2012.126>

833 Mays, K.L., Shepson, P.B., Stirm, B.H., Karion, A., Sweeney, C., Gurney, K.R., 2009. Aircraft-  
834 Based Measurements of the Carbon Footprint of Indianapolis. *Environ. Sci. Technol.* 43,  
835 7816–7823. <https://doi.org/10.1021/es901326b>

836 McKain, K., Down, A., Raciti, S.M., Budney, J., Hutyra, L.R., Floerchinger, C., Herndon, S.C.,  
837 Nehr Korn, T., Zahniser, M.S., Jackson, R.B., Phillips, N., Wofsy, S.C., 2015. Methane  
838 emissions from natural gas infrastructure and use in the urban region of Boston,  
839 Massachusetts. *Proc. Natl. Acad. Sci.* 201416261.  
840 <https://doi.org/10.1073/pnas.1416261112>

841 Miskell, G., Salmond, J., Alavi-Shoshtari, M., Bart, M., Ainslie, B., Grange, S., McKendry, I.G.,  
842 Henshaw, G.S., Williams, D.E., 2016. Data Verification Tools for Minimizing  
843 Management Costs of Dense Air-Quality Monitoring Networks. *Environ. Sci. Technol.*  
844 50, 835–846. <https://doi.org/10.1021/acs.est.5b04421>

845 Mitchell, L.E., Lin, J.C., Bowling, D.R., Pataki, D.E., Strong, C., Schauer, A.J., Bares, R., Bush,  
846 S.E., Stephens, B.B., Mendoza, D., Mallia, D., Holland, L., Gurney, K.R., Ehleringer,  
847 J.R., 2018. Long-term urban carbon dioxide observations reveal spatial and temporal

848 dynamics related to urban characteristics and growth. *Proc. Natl. Acad. Sci.* 115, 2912–  
849 2917. <https://doi.org/10.1073/pnas.1702393115>

850 Oakes, M.M., Burke, J.M., Norris, G.A., Kovalcik, K.D., Pancras, J.P., Landis, M.S., 2016.  
851 Near-road enhancement and solubility of fine and coarse particulate matter trace elements  
852 near a major interstate in Detroit, Michigan. *Atmos. Environ.* 145, 213–224.  
853 <https://doi.org/10.1016/j.atmosenv.2016.09.034>

854 Park, Y.M., Kwan, M.-P., 2017. Individual exposure estimates may be erroneous when  
855 spatiotemporal variability of air pollution and human mobility are ignored. *Health Place*  
856 43, 85–94. <https://doi.org/10.1016/j.healthplace.2016.10.002>

857 Pataki, D.E., Bowling, D.R., Ehleringer, J.R., 2003. Seasonal cycle of carbon dioxide and its  
858 isotopic composition in an urban atmosphere: Anthropogenic and biogenic effects. *J.*  
859 *Geophys. Res.-Atmospheres* 108, 1–8. <https://doi.org/10.1029/2003jd003865>

860 Patarasuk, R., Gurney, K.R., O’Keeffe, D., Song, Y., Huang, J., Rao, P., Buchert, M., Lin, J.C.,  
861 Mendoza, D., Ehleringer, J.R., 2016. Urban high-resolution fossil fuel CO<sub>2</sub> emissions  
862 quantification and exploration of emission drivers for potential policy applications. *Urban*  
863 *Ecosyst.* 19, 1013–1039. <https://doi.org/10.1007/s11252-016-0553-1>

864 Pfister, G.G., Walters, S., Lamarque, J.-F., Fast, J., Barth, M.C., Wong, J., Done, J., Holland, G.,  
865 Bruyère, C.L., 2014. Projections of future summertime ozone over the U.S. *J. Geophys.*  
866 *Res. Atmospheres* 2013JD020932. <https://doi.org/10.1002/2013JD020932>

867 Pouliot, G., Pierce, T., Denier van der Gon, H., Schaap, M., Moran, M., Nopmongcol, U., 2012.  
868 Comparing emission inventories and model-ready emission datasets between Europe and  
869 North America for the AQMEII project. *Atmos. Environ., AQMEII: An International*  
870 *Initiative for the Evaluation of Regional-Scale Air Quality Models - Phase 1* 53, 4–14.  
871 <https://doi.org/10.1016/j.atmosenv.2011.12.041>

872 Salt Lake City Corporation, 2016. A Joint Resolution of the Salt Lake City Council and Mayor  
873 Establishing Renewable Energy and Carbon Emissions Reduction Goals for Salt Lake  
874 City.

875 Shusterman, A.A., Teige, V.E., Turner, A.J., Newman, C., Kim, J., Cohen, R.C., 2016. The  
876 BErkeley Atmospheric CO<sub>2</sub> Observation Network: initial evaluation. *Atmos Chem Phys*  
877 16, 13449–13463. <https://doi.org/10.5194/acp-16-13449-2016>

878 Snyder, E.G., Watkins, T.H., Solomon, P.A., Thoma, E.D., Williams, R.W., Hagler, G.S.W.,  
879 Shelow, D., Hindin, D.A., Kilaru, V.J., Preuss, P.W., 2013. The Changing Paradigm of  
880 Air Pollution Monitoring. *Environ. Sci. Technol.* 47, 11369–11377.  
881 <https://doi.org/10.1021/es4022602>

882 Steenburgh, W.J., Massey, J.D., Painter, T.H., 2012. Episodic Dust Events of Utah’s Wasatch  
883 Front and Adjoining Region. *J. Appl. Meteorol. Climatol.* 51, 1654–1669.  
884 <https://doi.org/10.1175/JAMC-D-12-07.1>

885 Thompson, J.E., 2016. Crowd-sourced air quality studies: A review of the literature & portable  
886 sensors. *Trends Environ. Anal. Chem.* 11, 23–34.  
887 <https://doi.org/10.1016/j.teac.2016.06.001>

888 UDOT, 2017. Annual Average Daily Traffic (AADT) [WWW Document]. URL  
889 <https://www.udot.utah.gov/main/f?p=100:pg:0:::V,T:,528> (accessed 3.2.17).

890 U.S. EPA, 2016. Locomotives: Exhaust Emission Standards (No. EPA-420-B-16-024).

891 U.S. EPA, 2013. Integrated Science Assessment (ISA) of Ozone and Related Photochemical  
892 Oxidants (No. EPA/600/R-10/076F). Washington, DC.

893 Utah DEQ, 2018. Utah Winter Fine Particulate Study (UWFPS) [WWW Document]. URL  
894 [https://deq.utah.gov/legacy/programs/air-quality/research/projects/northern-ut-air-](https://deq.utah.gov/legacy/programs/air-quality/research/projects/northern-ut-air-pollution/winter-fine-particulate-aircraft-study.htm)  
895 [pollution/winter-fine-particulate-aircraft-study.htm](https://deq.utah.gov/legacy/programs/air-quality/research/projects/northern-ut-air-pollution/winter-fine-particulate-aircraft-study.htm) (accessed 4.3.18).  
896 Van den Bossche, J., Peters, J., Verwaeren, J., Botteldooren, D., Theunis, J., De Baets, B., 2015.  
897 Mobile monitoring for mapping spatial variation in urban air quality: Development and  
898 validation of a methodology based on an extensive dataset. *Atmos. Environ.* 105, 148–  
899 161. <https://doi.org/10.1016/j.atmosenv.2015.01.017>  
900 Venkatram, A., Isakov, V., Seila, R., Baldauf, R., 2009. Modeling the impacts of traffic  
901 emissions on air toxics concentrations near roadways. *Atmos. Environ.* 43, 3191–3199.  
902 <https://doi.org/10.1016/j.atmosenv.2009.03.046>  
903 Whiteman, C.D., Hoch, S.W., Horel, J.D., Charland, A., 2014. Relationship between particulate  
904 air pollution and meteorological variables in Utah’s Salt Lake Valley. *Atmos. Environ.*  
905 94, 742–753. <https://doi.org/10.1016/j.atmosenv.2014.06.012>  
906 Young, J.S., Whiteman, C.D., 2015. Laser Ceilometer Investigation of Persistent Wintertime  
907 Cold-Air Pools in Utah’s Salt Lake Valley. *J. Appl. Meteorol. Climatol.* 54, 752–765.  
908 <https://doi.org/10.1175/JAMC-D-14-0115.1>  
909 Zhao, C.L., Tans, P.P., 2006. Estimating uncertainty of the WMO mole fraction scale for carbon  
910 dioxide in air. *J. Geophys. Res. Atmospheres* 111, D08S09.  
911 <https://doi.org/10.1029/2005JD006003>  
912 Zimmerman, N., Presto, A.A., Kumar, S.P.N., Gu, J., Hauryliuk, A., Robinson, E.S., Robinson,  
913 A.L., Subramanian, R., 2017. Closing the gap on lower cost air quality monitoring:  
914 machine learning calibration models to improve low-cost sensor performance. *Atmos*  
915 *Meas Tech Discuss* 2017, 1–36. <https://doi.org/10.5194/amt-2017-260>  
916 Zivin, J.G., Neidell, M., 2018. Air pollution’s hidden impacts. *Science* 359, 39–40.  
917 <https://doi.org/10.1126/science.aap7711>  
918